Sperm fertility in mice with oligo-astheno-teratozoospermia restored by in vivo injection and electroporation of naked mRNA

Charline Vilpreux, Guillaume Martinez, Magali Court, Florence Appaix, Jean-Luc Duteyrat, Maxime Henry, Julien Vollaire, Camille Ayad, Altan Yavz, Lisa de Macedo, et al.

Sperm fertility in mice with oligo-astheno-teratozoospermia restored by *in vivo* injection and electroporation of naked mRNA

Charline Vilpreux[1], Guillaume Martinez[1,4], Paul Fourquin[1] Magali Court[1], Florence Appaix[6], Jean-Luc Duteyrat[2], Maxime Henry[7], Julien Vollaire[7], Camille Ayad[3], Altan Yavz[3], Lisa De Macedo[1], Geneviève Chevalier[1], Emeline Lambert[1], Sekou Ahmed Conte[1], Zeina Wehbe[1,4], Elsa Giordani[1], Véronique Josserand[7], Jacques Brocard[2], Coutton Charles[1,4], Bernard Verrier[3], Pierre F. Ray[1,5], Corinne Loeuillet[1], Christophe Arnoult[1] and Jessica Escoffier[1*].

[1] Université Grenoble Alpes, Inserm U1209, CNRS UMR 5309, Team Genetic, Epigenetic and Therapies of infertility, Institute for Advanced Biosciences 38 000 Grenoble, France

[2] Université Claude Bernard Lyon 1, CNRS UAR3444, Inserm US8, ENS de Lyon, SFR Biosciences, Lyon 69007, France

[3]Université Claude Bernard Lyon 1 - Laboratoire de Biologie Tissulaire et d'Ingénierie Thérapeutique, UMR 5305, Université Lyon 1, CNRS, IBCP, Lyon, France

[4] UM de Génétique Chromosomique, Hôpital Couple-Enfant, CHU Grenoble Alpes, Grenoble, France.

[5] UM GI-DPI, CHU Grenoble Alpes, Grenoble, France.

[6] Université Grenoble Alpes, Inserm U1209, CNRS UMR 5309, plateforme microcell, Institute for Advanced Biosciences 38 000 Grenoble, France

[7] Université Grenoble Alpes, Inserm U1209, CNRS UMR 5309, plateforme Optimal, Institute for Advanced Biosciences 38 000 Grenoble, France

* To whom correspondence should be addressed: Jessica Escoffier, Team "Genetics, Epigenetics and Therapies of Infertility", Institute for Advanced Biosciences (IAB), INSERM 1209, CNRS UMR 5309 University Grenoble Alpes, Grenoble, FRANCE.
Contact:mail to jessica.escoffier@univ-grenoble-alpes.fr
tel: 33 (0)4 76 63 71 11

Ethics statement

All procedures involving animals were performed in line with the French guidelines for the use of live animals in scientific investigations. The study protocol was approved by the local ethics committee (ComEth Grenoble # 318) and received governmental authorization (ministerial agreement # 38109-2022072716142778).

Abstract

Oligo-astheno-teratozoospermia (OAT), a recurent cause of male infertility, is the most frequent disorder of spermatogenesis with a probable genetic cause. Patients and mice bearing mutations in the *ARMC2* gene have a decreased sperm concentration, and individual sperm show multiple morphological defects and a lack of motility – a canonical OAT phenotype. Intracytoplasmic sperm injection (ICSI) is required to treat such a condition but it is associated with a small increase in birth defects in comparison to pregnancies not involving assisted conception . Consequently, new targeted treatments are needed to restore fertility. Here, a combination of *in vivo* injection and electroporation of capped and poly-A-tailed naked mRNA is tested as a strategy to treat *ARMC2*-related infertility in mouse. mRNAs coding for several reporter genes are tested and the efficiency and the kinetic of expression are assessed using *in vivo* and *in vitro* 2D and 3D imaging experiments. We show that mRNA-coded reporter proteins are detected for up to 3 weeks in germ cells, making the use of mRNA possible to treat infertility. We compare these results with those obtained with a non-integrative plasmid Enhanced Episomal Vector (EEV), which induces low and transient expression in spermatogenic cells. Consequently, injection and electroporation of naked mRNA-*Armc2* into the testes of *Armc2*-deficient males were performed and we show the presence of normal and motile sperm in the epididymis. These motile sperm were able to produce embryos by IVF and ICSI. This study shows for the first time that mRNA-*Armc2* efficiently restores fertility and opens new paths for male infertility treatment.

Key words: Sperm cells, infertility, protein therapy, mRNA, EEV, *In Vivo* Microinjection and Electroporation, *in vivo* imaging, Whole Testis Optical clearing, light sheet microscopy.

Introduction

Worldwide, 10-15 % of couples (or 70 million) face infertility [1]. Infertility is thus a major public health issue presenting significant medical, scientific and economic challenges (a multibillion € annual market)[2]. A significant proportion of infertilities is due to altered gametogenesis, where the sperm and eggs produced are incompatible with fertilization and/or embryonic development [3]. Approximately 40 % of cases of infertilities involve a male factor, either exclusively, or associated with a female deficiency [4].

Male gametogenesis, or spermatogenesis, is a highly complex physiological process which can be split into three successive steps: proliferation (mitosis of spermatogonia), reduction of the number of chromosomes (meiosis of spermatocytes), and morphogenesis of spermatozoa (spermiogenesis). The whole process involves around two thousands of genes, 60 % of which are expressed exclusively in the testes [5]. Because of this multiplicity of genes, spermatogenesis is strongly affected by genetic factors [5], with most severe disorders likely to be of genetic origin.

Among infertility disorders, oligo-astheno-teratozoospermia (OAT) is the most frequent (50 % [6]) and it is likely to be of genetic origin. Spermatocytograms of OAT patients show a decrease in sperm concentration, multiple morphological defects and defective motility [7, 8]. Because of these combined defects, patients are infertile and can only conceive by intracytoplasmic sperm injection (ICSI).

ICSI can efficiently overcome the problems faced. Nevertheless, concerns persist regarding the potential risks associated with this technique, including blastogenesis defect, cardiovascular defect, gastrointestinal defect, musculoskeletal defect, orofacial defect, leukemia, central nervous system tumors, and solid tumors [9-12]. Statistical analyses of birth records have demonstrated an elevated risk of birth defects, with a 30-40 % increased likelihood in cases involving ICSI [9-12], and a prevalence of birth defects between 1 % and 4 % [11]. To overcome these drawbacks, a number of experimental strategies have been proposed to bypass ARTs and restore spermatogenesis and fertility, including gene therapy [13-16].

Gene therapy consists of introducing a DNA sequence into the genome to compensate for a defective gene. It can thus rescue production of a missing protein, and is now applied both in research [17] and for the treatment of human diseases [18] .

Given the genetic basis of male infertility, the first strategy, tested in mice, was to overcome spermatogenic failure associated with monogenic diseases by delivery of an intact gene to deficient germ cells [13]. Gene therapy is effective in germ cells, as numerous publications have shown that conventional plasmids can be transferred into spermatogonia in several species with success, allowing their transcription in all cells of the germinal lineage [13-16]. Most experiments were performed in mouse models, delivering DNA constructs into living mouse germ cells by testis electroporation after microinjection of a DNA-containing solution into the seminiferous tubules. Using this method, it was possible to rescue meiosis and fertility in mouse models of infertility [13, 16]. However, the genetic changes induced are transmitted to any descendants. Consequently, gene therapy cannot be used to treat infertility in humans, both for ethical reasons and to avoid any eugenic deviations, and currently transmissible changes in humans are illegal in 39 countries [19]. Furthermore, the genetic modification of germ cell lines poses biological risks, including the induction of cancer, off-target effects, and cell mosaicism. Errors in editing may have adverse effects on future generations. It is exceedingly challenging to anticipate the consequences of genetic mosaicism, for instance, in a single individual [20, 21]. Gene therapies have thus raised both ethical controversy and long-term safety issues.

For these reasons, we decided to test an alternative strategy to DNA transfection based on the use of naked mRNA. Thanks to this change, the risk of genomic insertion is avoided, and thus there is no question of heritable alterations [22].The first part of this study presents a characterization of the protein expression patterns obtained following transfection of naked mRNA coding for reporter genes into the testes of mice. The second part is to apply the protocol to a preclinical mouse model of OAT. Patients and mice carrying mutations in the *ARMC2* gene present a canonical OAT phenotype and are infertile. The preclinical *Armc2* deficient (*Armc2* KO) mouse model is therefore a valuable model to assess whether *in vivo* injection of naked mRNA combined with electroporation can restore spermatogenesis. We chose this model for several reasons: first, *Armc2* KO mice are sterile and all sperm exhibit short, thick or coiled flagella [13]. As a result, 100 % of sperm are immobile, thus it should be

easy to determine the efficacy of the technique by measuring sperm motility with a CASA system. Second, the *Armc2* gene codes for an 867-amino acid protein and this large size represents a challenge for expression in the testis following electroporation.

To determine the efficacy of naked mRNA transfection as a method to achieve protein expression in the testes, we first assessed the level of transcription of reporter proteins after mRNA injection compared to the injection of a non-integrating plasmid, the Enhanced Episomal Vector (EEV). EEV is a vector derived from Epstein-Barr virus, it includes an origin of replication (EBV Ori) and the EBNA1 protein. Both elements, allows the synchronous initiation of extra-chromosomal EEV replication with host DNA at each S phase of the cell cycle and the segregation of the EEV episome in daughter cells. It is notable that EEV is maintained at a rate of 90-95% per cell division. It does not integrate or modify the host genome [11, 12].

In the present *in vivo* work, we injected and electroporated three distinct mRNAs coding for the following reporter proteins: green fluorescent protein (GFP), luciferase (Luc) and mCherry, and an EEV episome vector containing the sequences coding for both GFP and luciferase reporter proteins. The initial step was to characterize and validate the method of injection in adult males. Subsequently, the kinetics and patterns of expression of the electroporated mRNAs and EEV were compared using a variety of methods, including whole testis imaging, *in vivo* bioluminescence imaging, and tissue clearing. Subsequently, the mRNA transfection protocol was tested in a preclinical mouse model of OAT with the objective of restoring fertility.

Materials and methods

Animals

All procedures involving animals were performed in line with the French guidelines for the use of live animals in scientific investigations. The study protocol was approved by the local ethics committee (ComEth Grenoble # 318) and received governmental authorization (ministerial agreement # 38109-2022072716142778).

The animals used were (a) B6D2 F1 hybrid (♀ C57BL/6JRj crossed with ♂ DBA/2, Janvier laboratories; France) adult male mice aged between 8 and 25 weeks, (b) the *Armc2* KO mouse

strain obtained by CRISPR-Cas9 [23] and (c) CD1 female 6 weeks old (Janvier laboratories, Le Genest-Saint-Isle ,France). Experiments were carried out on wild type (WT) or *Armc2* KO adult male mice aged between 8 and 15 weeks.

Chemicals and reagents

Fast Green (FG) (F7258 – 25 g), phosphate buffered saline (PBS, D853 7- 500 mL), hematoxylin (GH5316 – 500 mL), eosin (HT110216 – 500 mL), terbutanol (471712 – 100 mL), Histodenz (D2158 – 100 g), sorbitol (S1876 – 100 g), urea (U5128 – 500 g), Potassium Phosphate, Monobasic (P0662), Magnesium Sulfate (anhydrous) (M9397), Sodium Bicarbonate Calcium Chloride · 2H2O (22317), EDTA (E9884), Sodium Lactate (60 % syrup - d= 1,32 g L^{-1}) (L7900), Glucose (G8270), Penicillin (P4333), Streptomycin (P4333), HEPES (H0887), PVA 30,000-70,000 (P8136), Albumin, Bovine Fraction V (A3803), M2 medium (M7167), Hyaluronidase (H3884), mineral oil (M8410), PolyVinylPyrolidone (PVP360-100G), M16 medium (MR-016) and Collagenase (C8176) were purchased from Sigma Aldrich (Saint-Quentin-Fallavier, France). Sodium Chloride (1112-A) were purchased from Euromedex (Souffelweyersheim, France). Potassium Chloride (26764) L-Glutamine (35050038), Sodium Pyruvate (11360039), NEAA (11140050) and EAA (11130036) were purchased from Life Technologies, (Waltham, MA USA). Schorr staining solution was obtained from Merck (Darmstadt, Germany). Mfel HF (R35895) and RNase-free DNase I (M03035) were obtained from New England Biolabs (Ipswich, MA, USA). Paraformaldehyde (PFA, 15710) was obtained from Electron Microscopy Science (Hatfield, PA, USA). Ketamine and xylazine were obtained from Centravet (Dinan, France). Fluorescent i-particles (NIRFiP-180) were obtained from Adjuvatis (Lyon, France). Script Gurad RNAse CleanCap AG (040N-7113-1), CleanCAp *EGFP*-mRNA (040L-7601-100), T7-FlashScribe kit (C-ASF3507), poly(A) tail (C-PAP5104H) and CleanCap *Luciferase*-mRNA (L-7602-1000) were obtained from Tebubio (Le Perray en Yvelines, France).

Plasmids

All plasmid, EEV *CAGs-GFP-T2A-Luciferase*, (EEV604A-2; System Bioscience, Palo Alto, CA, USA), mCherry plasmid (given by Dr. Conti MD at UCSF, San Francisco, CA, USA) and EEV-*Armc2-GFP* plasmid (CUSTOM-S017188-R2-3, Trilink, San Diego, CA, USA) were amplified by bacterial transformation (E. coli, EC0112; Thermo Fisher, Courtaboeuf, France). After expansion, plasmids were purified with a NucleoBond Xtra Midi kit (740410-50; Macherey-

Nagel, Düren, Germany) using manufacturer's protocol. All plasmids DNA pellets were solubilized in (DNAse- and RNAse-free) milliQ water (Sigma Aldrich, Saint-Quentin-Fallavier, France), before used.

The EEV *CAGs-GFP-T2A-Luciferase* episome contains the cDNA sequences of Green Fluorescent Protein (GFP) and luciferase, under the control of a CAGs promoter (Supp Fig 1). After purification, the EEV *CAGs-GFP-T2A-Luciferase* plasmid concentration was adjusted to 9 µg μL^{-1}. Prior to injection, 3.3 µL of this plasmid solution was mixed with 1 µL 0.5 % Fast Green and 5.7 µL sterile PBS to obtain a final EEV concentration of 3 µg μL^{-1}. The EEV-*Armc2-GFP* plasmid contains the mouse cDNA sequences of *Armc2 (ENSMUST00000095729.11)* and the Green Fluorescent Protein (GFP) genes under the control of a strong CAGs promoter (Supp Fig 1). After amplification and purification, the final plasmid concentration was adjusted to 9 µg μL^{-1} in water. Prior to injection, 3.3 µL of this plasmid solution was mixed with 1 µL of 0.5 % Fast Green and 5.7 µL of sterile PBS to obtain a final EEV concentration of 3 µg μL^{-1}. The mcherry plasmid contains the cDNA sequence of *mCherry* under the control of CMV and T7 promoters (Supp Fig 1). After amplification and purification, the final plasmid concentration was adjusted to 9 µg μL^{-1}.

Armc2-mRNA

Armc2-mRNA used for *in vivo* testes microinjection and electroporation was obtained from Trilink (San Diego, CA, USA). The commercial *Armc2*-mRNA has an AG CleanCap, a poly(A) tail of 120 adenosines and 3 HA-FLAG. The main challenge with mRNA-based therapy is mRNA stability. To improve mRNA stability *in vivo* and avoid its degradation by ribonucleases, optimization techniques were implemented. Thus, the used mRNA has codon optimization, a poly(A) tail and a CleanCap. To verify the efficiency of cell transfection, an *EGFP*-mRNA was injected together with the *Armc2*-mRNA. During the injection, the concentration of *EGFP*-mRNA and *Armc2*-mRNA were 300 ng μL^{-1} each.

mcherry*-mRNA transcription *in vitro

The circular *mCherry* plasmid was linearized using the restriction enzyme MfeI HF at 37 °C for 1 h. The pm-*mCherry* was then extracted and purified with the DNA Clean and Concentrator-25 ™ kit (D4033; Zymo Research, Irvine, CA, USA). The pm-*mCherry* was subsequently transcribed in vitro using the T7-FlashScribe kit (C-ASF3507; Tebubio, Le Perray en Yvelines,

France). The mRNA was capped with a clean cap (CleanCap AG; 040N-7113-1, Tebubio, Le Perray en Yvelines, France), and a poly(A) tail (C-PAP5104H; Tebubio, Le Perray en Yvelines, France) was added before purification using the NucleoSpin RNA Clean Up kit (740948-50; Macherey-Nagel, Düren, Germany). Prior to injection, *mcherry*-mRNA was mixed with Fast Green to obtain a final concentration of 300 ng μL^{-1} (0.05 % FG, PBS).

Agarose gel electrophoresis of the Episomal Vector EEV and mRNA-mCherry

Before loading on a pre-stained (Gel Green) 1.5 % agarose gel, the EEV-plasmid and mRNA were mixed with a loading dye (Promega Blue Orange G1904, Promega, Charbonnières France). An aliquot of each sample (500 ng) was loaded into each well and electrophoresis was performed for 30 min at 100 V at room temperature (RT). A DNA size marker (Gene ruler SM1331, Thermo Scientific, Courtaboeuf, France) was used to assess molecular weight. Gel images were acquired using a ChemiDoc XRS+ (BIORAD, Marnes-la-Coquette, France).

***In vivo* microinjection and electroporation of testes**

Electroporation was conducted as previously described [15]. Briefly, male mice B6D2, *Armc2*$^{+/+}$ or *Armc2*$^{-/-}$, depending of the experimental conditions, were anesthetized with ketamine/xylazine solution (100 mg μL^{-1} and 10 mg μL^{-1} respectively). The testes were pulled out from the abdominal cavity or scrotum. Under a binocular microscope and using microcapillaries pipettes (FemtoTip II ®, Eppendorf, Montesson, France), 10 µL DNA (3 µg μL^{-1} - 0.05 % FG) or mRNA (300 ng μL^{-1} -0.05 % FG) was injected into the seminiferous tubules through the *rete testis* applying a constant pressure (microinjector, Femto Jet 4i, Eppendorf, Montesson, France). Two series of 8 square electric pulses (25 V for 50 ms) were applied to the testis using tweezer-type electrodes linked to an electroporator (Gemini, BTX, Holliston, MA, USA). The testes were then replaced in the abdominal cavity, and the abdominal wall and skin were sutured. For each animal, the left testis was injected and electroporated with the different nucleic acids (mRNA, EEV), whereas the right testis was injected with a control solution (PBS, 0.5 % FG) as a control. Both testes were electroporated.

Flash Freezing and Fluorescence Analysis of testes

Depending on the experimental condition, 1-, 3- or 7-days post injection, the testes were collected and washed for 5 min in PBS. Then, they were embedded in Peel-A-Way Cryomolds

filled with OCT Mounting media (VWR, Rosny-sous-Bois, France). The samples were flash frozen in a 100 % isopentane solution (524391; Carlo ERBA, Val-de-Reuil, France), pre-cooled with liquid nitrogen. Once frozen, they were cut into 20 µm sections using a cryostat. The cryostat sections were then fixed with 4 % PFA-PBS for 10 min at 4 °C and counterstained with 1.8 µM DAPI (nuclear stain) before observation using an Axioscan Z1 slide scanner or a confocal AxioObserver Z1 multiparameter microscope LSM710 NLO – LIVE7 – Confocor 3. The fluorescence of the different reporter proteins was detected using appropriate filters for DAPI, GFP, Texas Red (for mCherry), and Cy7 (for the Fluorescent i-particles NIRFiP-180).

Tissue collection and histological analysis

For histological analysis, treated and control B6D2 testes were fixed by immersion in 4 % paraformaldehyde (PFA) for 14 h. They were then embedded in paraffin before cutting into 5 µm sections using a microtome (Leica biosystems, Wetzlar, Germany). After deparaffination, the sections were stained with hematoxylin and eosin. Stained sections were digitized at 20x magnification using an axioscan Z1-slide scanner (Zeiss, Léna, Germany). Spermatogenesis was assessed by measuring the area of seminiferous tubules and the cross sections of round tubules (μm^2) ($n > 35$ tubules per testis section; n=5 testis sections per condition). Statistical significance of differences was determined using a Student's *t*-test.

***Ex vivo* Fluorescence Analysis**

To analyze the expression of the reporter proteins GFP and mCherry in seminiferous tubules, whole testes were examined under an inverted microscope (CKX53, Olympus, Shinjuku, Tokyo, Japan). Exogenous fluorescence was detected using filters for GFP and Texas Red.

Harris-Shorr sperm Analysis

Sperm were collected from the caudae epididymides of mice (Control, injected with EEV-*GFP*, *GFP*-mRNA, or *Armc2*-mRNA). They were allowed to swim for 10 min at 37 °C in 1 mL M2 media. Sperm were centrifuged at 500 g, washed once with PBS, and fixed 4 % paraformaldehyde in PBS for 1 min at RT. After washing with 1 mL acetate ammonia (100 mM), the sperm suspensions were spotted onto 0.1 % poly L-lysine precoated slides (Thermo Scientific, Courtaboeuf, France) and left to dry. Harris–Schorr staining was then performed according to the WHO protocol [24], and at least 150 sperm were analyzed per animal.

Whole Testis Optical clearing and 3D image reconstructions

Optical clearing (adapted from uDISCO and Fast 3D clear protocols)

Adult mice were euthanized by cervical dislocation and then transcardiac perfused with 1X PBS (Sigma Aldrich, Saint-Quentin-Fallavier, France). The testes were extracted and fixed for two days at 4 °C in 4 % PFA (Electron Microscopy Sciences, Hatfield, PA ,USA). Samples were then washed with PBS for at least two days. Mouse testes were subsequently dehydrated in graded series of tert-butanol solutions (Sigma Aldrich, Saint-Quentin-Fallavier, France) at 35 °C as follows: 30 % overnight (O/N), 50 % for 24 h, 70 % for 10 h, 80 % O/N, 90 % for 10 h, 96 % O/N, and 100 % for 10 h. The testes were cleared in clearing solution (96 % Histodenz,2 % Sorbitol ,20 % Urea) for 2 days. Then, nuclei were stained with 3.6 μM DAPI (20 % DMSO; 2 % Triton, 1 % BSA) for 2 days. Finally, the testes were then conserved in the clearing solution at 4°C until observation by microscopy. All these steps were carried out under agitation and protected from light.

3D tissue Imaging

The optically-cleared mouse testes were imaged on a lightsheet fluorescence microscope (Blaze, Miltenyi Biotec, Germany), using a 4x NA 0.35 MI PLAN objective protected by a dipping cap for organic solvents, with an overall working distance of 15 mm. Acquisitions on the horizontal plane were obtained with a fixed lightsheet thickness of 3.9 µm at both 488 nm and 561 nm with no overlap between horizontal planes. Voxel resolution x = 1.21; y = 1.21; z = 2 µm. 3D reconstructions were created using Imaris software (Oxford Instruments plc, Abingdon, UK).

Cellular image analysis

The optically-cleared mouse testes were imaged using a 'ConfoBright' system which is a unique adaptive confocal microscope (Nikon A1R MP, Nikon Europe B.V., The Netherlands) equipped with a deformable mirror module (AOS-micro, AlpAO, Montbonnot, France) for the correction of geometrical aberrations. Indeed, the deep confocal imaging of the cleared 3D sample requires long distance objectives and immersion media of different refractive index, resulting in optical aberrations. Images were acquired using Adaptive Optics optimization with an apo LWD 40x/1.15 water immersion objective (WD 600 µm) and a 10x/0.45 objective. FIJI

295 software (Opened source software) was used to process and analyze images and Imaris
296 software for the 3D reconstructions.

297 **Bioluminescence imaging**

298 *In vivo* Bioluminescence imaging was performed at several time points after *in vivo Luciferase*
299 -mRNA or EEV-*GFP-luciferase* injection and electroporation (n=5 mice per condition). Ten
300 minutes before imaging, mice received an intraperitoneal injection of 150 µg g^{-1} of D-luciferin
301 (Promega, Charbonnières France), and were then anesthetized (isoflurane 4 % for induction
302 and 1.5 % for maintenance) before placing in the optical imaging system (IVIS Lumina III,
303 PerkinElmer, Courtaboeuf, France). *In vivo* bioluminescence signals were measured in selected
304 regions of interest (injected testes) and were expressed as mean photons per second (mean
305 ± SEM). Background bioluminescence was measured on images from control mice. When the
306 *in vivo* bioluminescence signal was no longer detectable, testes were collected and immersed
307 in a luciferin solution for a few minutes before performing *ex vivo* imaging to confirm the
308 absence of signal.

309 **Sperm motility**

310 The cauda epididymis was dilacerated in 1 mL of M2 medium (Sigma Aldrich, Saint-Quentin-
311 Fallavier, France) and spermatozoa were allowed to swim out for 10 min at 37 °C. After
312 incubation, 30 µl of the sperm suspension was immediately placed onto analysis chamber (2X-
313 CEL Slides, 80 µm depth, Leja Products B.V., The Netherlands) kept to 37°C for microscopic
314 quantitative study of sperm movement. Motility of the spermatozoa was evaluated at 37°C
315 with an Olympus microscope and Computer Aided Sperm Analysis (CASA) (CEROS II apparatus;
316 Hamilton Thorne, Beverley, MA, USA). The settings employed for analysis were: acquisition
317 rate: 60 Hz; number of frames: 30; minimum contrast: 30; minimum cell size: 4; low-size gate:
318 0.13; high-size gate: 2.43; low-intensity gate: 0.10; high-intensity gate: 1.52; minimum
319 elongation gate: 5; maximum elongation gate: 100; magnification factor: 0.81.

320 The motility parameters measured were: straight line velocity (VSL); curvilinear velocity (VCL);
321 averaged path velocity (VAP); amplitude of lateral head displacement (ALH); beat cross
322 frequency (BCF); linearity (LIN); straightness (STR). Hyperactivated sperm were characterized
323 by VCL > 250 µm s^{-1} , VSL > 30 µm s^{-1}, ALH > 10 µm and LIN < 60, Intermediate by VCL >
324 120 µm s^{-1} and ALH > 10 µm, progressive sperm by VAP > 50 µm s^{-1} and STR > 70 % and slow
325 sperm by VAP < 50 µm $s^{-1}$and VSL < 25 µm s^{-1}.

Western blot

Western blotting was performed on HEK-293T cells (ATCC, Manassas, VA, USA) transfected with EEV-*Armc2* or *Armc2*-mRNA. Cells were transfected using JetPrime (101000027; Polyplus Illkirch, France) for DNA and JetMessenger (101000056; Polyplus Illkirch ,France) for mRNA vectors, both according to the supplier's recommendations. After 48 h, the cells were washed with PBS and scraped off before centrifuging at 4 °C, 1500 RPM for 5 min. The cell pellet was then resuspended in lysis buffer (87787; Thermo Scientific, Courtaboeuf, France) supplemented with an EDTA-free cocktail of protease inhibitors (11836170001; Roche, Bale, Swiss). The suspension was stirred at 4 °C for 2 h, and then centrifuged at 16,000 g at 4 °C for 10 min. The protein content of the supernatant was estimated with QuantiPro™ BCA Assay kit (Sigma Aldrich, Saint-Quentin-Fallavier, France) before adding 5X Laemmli + 5 % β-mercaptoethanol and heating at 95 °C for 10 min. For the Western blot, 30 µg of proteins were deposited on a ready-made Bis-Tris gel 12 % (Thermo Fisher, Courtaboeuf, France). After transfer, the PVDF membrane was blocked with 5 % milk in Tris-Buffered Saline solution containing 0.1 % Tween 20 (TTBS) before immunodetection. The anti HA antibody (11867423001; Sigma Aldrich, Saint-Quentin-Fallavier, France) was diluted in TTBS at 1/5000. After incubation with secondary antibodies (AP136P; Sigma Aldrich, Saint-Quentin-Fallavier, France) diluted at 1:10,000 in TTBS, binding was revealed with an enhanced chemiluminescence detection kit (1705062; Clarity Max Western ECL Substrate; BIORAD, Marnes-la-Coquette, France). Membranes were imaged on a ChemiDoc™ system (BIORAD, Marnes-la-Coquette, France).

Immunofluorescence

Immunofluorescence analysis of dissociated testicular cells was performed as follows. After collection, the tunica albuginea was removed from the testes. Then the tissue was mechanically separated with 18G needles. Once washed with PBS, the testicular cells were placed in a dissociation medium containing 1 mg collagenase type V /mL RPMI for 20 min at 37 °C. After filtration (100 µm filter) and centrifugation (5 min at 200 g) the pellets were resuspended in PBS before centrifugation once again. The pellet was then fixed in 1 mL PFA 4 % for 5 min. Then 10 mL of ammonium acetate (0.1 M) was added. Finally, 2 mL of medium was spread on a slide. Testicular cells were permeabilized with 0.1 % PBS-Triton X-100 for 20 min at room temperature. Slides were then blocked in 10 % BSA with PBS-Tween 0.1 % for

30 min before incubating overnight at 4 °C with primary antibodies anti-rabbit *ARMC2* (1/50) (HPA053696, Sigma Aldrich, Saint-Quentin-Fallavier, France) and anti-guinea pig tubulin (1/100) (AA345, Swiss Institute of Bioinformatics, Lausanne, Swiss) diluted in PBS-Tween 0.1 % - 5 % BSA. Slides were washed with PBS before incubating for 1 h with secondary antibodies: anti-guinea pig (1/500) (A-11073, Thermo Fischer, Courtaboeuf, France) and anti-rabbit (1:1000) (A-11036, Thermo Fischer, Courtaboeuf, France). Samples were counterstained with DAPI and mounted with DAKO mounting media (NC2313308; Life Technology, Courtaboeuf, France). Fluorescence images were acquired under a confocal microscope (Zeiss, Jena, Germany) fitted with a 63× oil immersion objective. Images were analyzed with ZEN lite software (Zeiss, Jena, Germany).

Intra-cytoplasmic sperm injection (ICSI)

Collection of gametes for ICSI

Armc2$^{-/-}$ sperm or *Armc2*$^{-/-}$ rescued sperm were harvested by dilaceration of the cauda epididymis. They were allowed to swim for 10 min at 37°C in 1 ml of CZB.HEPES medium containing (in mM) (HEPES 20, NaCl 81.6, KCl 4.8, $MgSO_4$ 1.2, $CaCl_2$ 1.7, KH_2PO_4 1.2, EDTA.Na_2 0.1, Na-lactate 31, $NaHCO_3$ 5, Na-pyruvate 0.3, polyvinyl alcohol 0.1 mg mL^{-1}, phenol red 10 mg mL^{-1} (0.5 % (w/v) in DPBS), pH 7.4) KCl 125, NaCl 2.6, Na_2HPO_4 7.8, KH_2PO_4 1.4 and EDTA 3 (pH 7.0)).The sperm head was separated from the tail by applying multiple piezo pulses (PiezoXpert®, Eppendorf, Montesson, France)

Eggs preparation

CD1 female mice, 7 weeks old, were superovulated by IP injection of 7.5 IU pregnant mare's serum gonadotrophin (PMSG; Centravet, Dinan, France) followed by 7.5 IU HCG (Centravet, Dinan, France) 48 h later. Eggs were collected from oviducts about 14 h after HCG injection. Cumulus cells were removed with 0.1 % hyaluronidase in M2 medium for 5–10 min. Eggs were rinsed thoroughly and kept in KSOM medium containing (in g L^{-1}: NaCl 5.55, KCl 0.19, KH_2PO_4 0.05, $MgSO_4$ 0.05, $NaHCO_3$ 2.1, $CaCl_2 \cdot 2H2O$ 0.250, EDTA 0.004, L-Glutamine 0.146, Na-lactate 1.870, Na-pyruvate 0.020, Glucose 0.04, Penicillin 0.05, Streptomycin 0.07, BSA 1.000, NEAA 0.5 % and EAA 1 %.), at 15°C for at least 15 min until required for ICSI.

ICSI procedures

ICSI was performed according to the method described by Yoshida and Perry (2007)[25].For microinjection, *Armc2*$^{-/-}$ sperm or *Armc2*$^{-/-}$ -rescued motile sperm heads were separated from the tail by applying multiple piezo pulses (PiezoXpert®, Eppendorf, Montesson, France). Sperm heads were introduced into the ooplasm using micromanipulators (Micromanipulator InjectMan®, Eppendorf, Montesson, France) mounted on an inverted Nikon TMD microscope (Nikon, Minato-ku, Tokyo, Japan). Eggs that survived the ICSI procedure were incubated in KSOM medium at 37 °C under in an atmosphere of 5 % CO_2. Pronucleus formation was checked at 6 h after ICSI, and outcomes were scored up to the blastocyst stage.

In vitro fertilization (IVF).

Armc2$^{-/-}$ sperm or *Armc2*$^{-/-}$ rescued sperm were harvested by dilaceration of the cauda epididymis. They were allowed to swim in *IVF* well in capacitated in M16 + 4 % BSA at 37 °C for 10 minutes. Eggs were collected from mature CD1 females (6 weeks old) synchronized with 7.5 units of pregnant mare serum gonadotrophin (PMSG) and 7.5 units of human chorionic gonadotrophin (hCG) prior to collection. Cumulus were incubated for 10 minutes in 500 µL M16 (MR-016; Sigma Aldrich, Saint-Quentin-Fallavier, France) / 1mg L^{-1} collagenase (C8176, Sigma Aldrich). Cumulus-free and zona-free eggs were collected, and rinsed twice with 500 µl M16 medium. Eggs were incubated with either *Armc2*$^{-/-}$ sperm or *Armc2*$^{-/-}$ rescued sperm) in capacitated medium (37 °C, 5 % CO_2) for 4 hours. After incubation, unbound sperm were washed away and eggs were incubated with KSOM at 37 °C, 5 % CO_2. Twenty-four hours after fertilization, we scored the different stages (unfertilized oocytes, aborted embryos, and 2-cell embryos as an indication of successful fertilization).

Statistical analyses

Statistical analyses were performed using SigmaPlot (version 10; Systat Software, Inc., San Jose, CA, USA). To account for sample variability between animals, a paired t-test, Mann-whitney rank sum test, on-way Anova and Wilcoxon test were used. Data are displayed as mean ± SEM. P values of * ≤ 0.05, ** ≤ 0.01, or *** ≤ 0.001 were considered to represent statistically significant differences.

Results

1. ***In vivo*** **microinjection and electroporation of mouse testes**

Two routes have been described for microinjection of DNA into the testes: direct injection through the *tunica albuginea,* or injection into the lumen of the seminiferous tubules via the *rete testis*. We chose the *rete testis* route and evaluated the efficacy of the microinjection protocol. In particular, we wished to better characterize the diffusion of the injected solution in the volume of the testis, as we were unable to find any information on this parameter in the literature. The efficacy of microinjection *via rete testis* was assessed using fluorescent i-particles NIRFiP-180, and by measuring their diffusion in testis cross sections examined by microscopy 3 days post-injection (Fig 1). To avoid lesions due to overfilling, the injection was controlled by measuring the expansion of the staining of the peripheral seminiferous tubules during the injection. Injections were stopped when the testes were filled to 2/3 of their capacity (Fig 1A-B). In testis cross sections, the fluorescent i-particles NIRFiP-180 were heterogeneously distributed, and mainly observed in seminiferous tubules located in the peripheral region of the testes, with fewer particles present in the center of the testes (Fig 1C-D). Moreover, no fluorescent i-particles NIRFiP-180 were visible in the peritubular space. These results indicated that microinjection through the *rete testis* did not produce a homogenous distribution of the particles throughout the seminiferous tubules. Nevertheless, the seminiferous tubules remained intact, as no signal was observed in the peritubular space (Fig 1C-D).

Next, we assessed the overall safety of the *rete testis* microinjection and electroporation of mRNA and EEV into testes. The safety of the protocol was evaluated by comparing macroscopic and microscopic anatomies of control (injected with control solution, PBS, 0.05 % FG), and treated testes (injected either with EEV-*GFP* (PBS, 0.05 % FG) or *GFP*-mRNA (PBS, 0.05 % FG)). Three days post-injection, the testes were first observed under a binocular microscope to identify possible macroscopic degeneration of the seminiferous tubules (Fig 2 A1 and 2 B1). Degenerations appear as pearly white lesions at the surface of the testis as illustrated in Supp Fig 2 following over electroporation. With the protocol we have developed, no such lesions were observed. Next, the testes were measured and weighed. No statistical differences in length and weight were observed between control and treated testes (Fig 2 A2, A3, B2, B3). Then, microscopic differences were sought by histological analysis of 5 µm sections (Fig 2C). No difference was observed between the control condition and EEV-*GFP* or *GFP*-mRNA on the full cross sections (Fig 2 C1, C2, C3). Next, we observed all the different

testicular cells, including all germ cell types and Sertoli cells (Fig 2 D1, D2, D3) for each condition. The layered structure of germ cells was identical in in all conditions. Analysis of the histological sections revealed no differences in the tubules area of the testes injected either with EEV-*GFP* or *GFP*-mRNA (Fig 2 E). At last, Harris-Shorr staining of the epididymal sperm cells demonstrated that there were no increases in morphological defects when mRNA and EEV were used in comparison with the control (Fig 2 F4). Taken together, these results suggest that *in vivo* microinjection and electroporation of EEV or mRNA did not perturb spermatogenesis .

2. Analysis of EEV-*GFP* and *GFP*-mRNA testicular expression by whole testis imaging

After validating the injection method, we compared the kinetics of GFP expression and the maintenance of the fluorescent signals for mRNA and EEV. To do so, we injected and electroporated one testis of adult B6D2 mice with EEV-*GFP* (n=129) or with *GFP*-mRNA (n=65). At 0-, 1-, 7-, 15-, 21-, 28-, 35-, 42- and 49-days post-injection, the whole testes were observed under an inverted microscope. The exogenous fluorescence was directly visible at the surface of the testes when illuminated with light at the appropriate wavelength (Fig 3 and Fig 4). No testicular lesions were observed on the testes at any post injection time (Fig 3 A1-H1 and Fig 4 A1-F1). In addition, both *GFP*-mRNA and EEV-*GFP* induced GFP expression in the testes (Fig 3 A2-H2 and Fig 4 A2-F2). It is worth noting that both vectors induced GFP expression at one day post-injection. However, the durations of fluorescent signals were different. For EEV, GFP fluorescence was still observable on day 42 for 100 % of samples, and 56 % of samples were positive on day 49, indicating that expression lasted around 1.5 months (Fig 4G). In contrast, for mRNA, 100 % of testes were labelled on day 21, but none showed any fluorescence on day 28 (Fig 4G). Thus, EEV transfection allowed a considerably longer duration of expression than mRNA. (Fig 3 and 4). It is important to underline that the signal measured is the fluorescence emitted by the GFP. This signal is dependent of both the half-lives of the plasmid/mRNA and the GFP. Therefore, the kinetic of the signal persistence (which is called here expression) is a combination of the persistence of the vector and the synthetized protein. In addition to differences in duration of expression, the GFP expression patterns were clearly different: mRNA produced a large, diffuse pattern, highlighting the shape of the seminiferous tubules; EEV-*GFP* produced a punctiform pattern (Fig 3B and 4B.) These results suggest that *GFP*-mRNA

and EEV-*GFP* targeted different seminiferous cell types, such as Sertoli cells and all germline cells, or that there were differences in terms of transfection efficiency.

3. Kinetics of EEV and mRNA expression assessed by *in vivo* imaging.

To further assess and compare the kinetics of expression of the two vectors, we expressed exogenous luciferase in the testis using EEV or mRNA and observed the level of luciferase by *in vivo* bioluminescence imaging. For EEV, we took advantage of the fact that the EEV plasmids contains the DNA sequence of the luciferase protein (*CAGs-GFP-T2A-Luciferase*) in addition to the DNA sequence of the GFP fluorescent protein (Supp Fig 1). For mRNA, we injected commercial naked *luciferase*-mRNA into the *rete testis* according to the same protocol as used for *GFP*-mRNA. For this set of experiments, we injected the EEV-*GFP-Luc* and *luciferase*-mRNA into the testes of 6 adult mice on day 0. We injected a similar number of copies of mRNA and EEV. The testes were imaged *in vivo* to detect bioluminescence expression, on day 1 and weekly until disappearance of the signal, no more than 120 days post-injection (Fig 5). For EEV-*GFP-Luciferase*, the bioluminescence induced by transfection was detected from day 1. After a rapid decrease in signal intensity over the first 3 weeks, a weak but constant signal remained detectable for 3 months, then faded away (Fig 5 A1-A2). For *Luciferase*-mRNA, expression was also detected from day 1. The bioluminescence decreased gradually over 3 weeks, becoming undetectable thereafter (Fig 5B1-B2). These results are consistent with our previous results (Fig 3) and confirm that EEV allows a longer expression of exogenous protein within the testis. Fig 5C compare the kinetics of expression observed with EEV and mRNA. Overall, our results indicated stronger expression for mRNA than for EEV, but with expression decreasing rapidly over-time, and almost no remaining signal after 3 weeks. In contrast, residual expression was detectable for several months with EEV.

4. Assessing testicular and cellular *GFP*-mRNA expression using whole testicle optical clearing, light sheet microscopy, and 3D-microscopic reconstructions

To better characterize the spatial distribution of *GFP*-mRNA expression in the testis, we performed whole testicular optical clearing. On day 0, we injected and electroporated testes with *GFP*-mRNA (n=6). On day 1, we harvested the testes and cleared them with a modified optical clearing protocol, as described in the MM section. After complete clearing (Fig 6 A), we observed the testes under a light sheet microscope and performed 3D reconstruction (videos

1, 2 and Fig 6 B). From this 3D reconstruction, we determined the volume of testis stained with GFP. The testis was sliced into 500 stacks, and the volume occupied by GFP staining was estimated by measuring the GFP-positive area in each stack and multiplying it by the thickness of the stack (10 µm). Measurements were possible only for the first 250 stacks due to optical problems with the last 250 stacks. To overcome this problem, and acquire information for the whole testis, the sample was turned by 180 ° and the measures repeated. A total GFP-stained surface of 0.51 mm^3 and 0.23 mm^3 was determined for face 1 and face 2, respectively. The corresponding total volume for the 250 stacks was measured as 60 mm^3, therefore 0.81 % and 0.24 % of the testis volume was transfected for face 1 and face 2 respectively (Fig 6 B).

5. Assessing GFP cellular expression using whole testicle optical clearing and confocal microscopy

Because the GFP fluorescence patterns were different for the two nucleic vectors when observed under the inverted microscope (Fig 3), we wondered whether the same cell types were targeted in both cases. To address this question, the whole optical cleared testes from EEV-*GFP* and *GFP*-mRNA-transfected mice were observed under a confocal microscope. The different cell types were identified based on their positions within the seminiferous tubule, their cellular shape and their nuclear morphology - revealed by nuclear staining. For instance, Sertoli cells have an oval to elongated nucleus and the cytoplasm presents a complex shape ("tombstone" pattern) along the basement membrane [26]. Round spermatids have small, round and compact nuclei with a nucleolus and are localized between the spermatocytes and elongated spermatids [27]. For EEV-*GFP*, on day 1 post injection and electroporation, a strong punctiform green fluorescence was visible inside the seminiferous tubules (Fig 7 A). Based on the different morphological criteria, this fluorescent signal was detected in spermatocytes, round spermatids and Sertoli cells (Fig 7 BC). On day 7, the GFP signal induced by EEV-*GFP* was reduced and only isolated signals in a few seminiferous tubules (1 per 11 tubules) were observed (Fig 7 D). These signals were associated only with Sertoli cells only (Fig 7 E).

For the mRNA vector, on day 1 and day 7 post-injection and electroporation, an intense fluorescence was observed in all the germ cells and in Sertoli cells in the seminiferous tubules (Fig 8A). At the cellular level, this fluorescent signal was associated with spermatogonia, spermatocytes, round spermatids, elongated spermatids, and mature spermatids cells to similar extents for both post-injection times (Fig 8 B, D). In contrast to what was observed with

EEV on day 7, no reduction in the number of fluorescent seminiferous tubules was noted when using *GFP*-mRNA, with 8 out of 10 tubules stained (Fig 8 CD).

6. Expression of naked *mcherry*-mRNA in testis following electroporation

Heterologous expression is well known to depend on the protein studied, we therefore tested the same reporter proteins to compare the mRNA and EEV vectors in the experiments presented above. Apart from the bioluminescence experiments with luciferase, we compared only GFP protein expression. To validate and confirm the capacity of naked mRNA to express proteins in the testes after injection and electroporation, we further challenged the method with mCherry, another reporter protein (Supp Fig 1BD). We injected homemade naked mRNA coding for mCherry into the testes. As previously with *GFP*-mRNA, no testicular lesions were observed (Supp Fig 3 A1, B1, C1, D1, E1, F1).

The assessment of the temporal persistence of testicular mCherry fluorescent protein expression revealed a robust red fluorescence from day 1 post-injection, which remained detectable for at least 15 days (Supp Fig 3 B2, C2, and D2). At the cellular level, the fluorescent signal was detected in germ cells, including spermatogonia, spermatocytes, round spermatids, mature spermatids, and Sertoli cells on days 1 and 7 post-injection (Supp Fig 4).

Finally, we compared the kinetics and levels of expression of the three different mRNA molecules, coding for mCherry, GFP and luciferase. By comparing the number of mice expressing *mCherry*-mRNA, *GFP*-mRNA and *luciferase*-mRNA fluorescence/luminescence over 21 days, we observed first that expression was detectable for all mRNAs on day 1, and second that the duration of expression was slightly different for the individual mRNAs. For instance, on day 15, 100 %, 80 % and 60 % of mice injected with *GFP*-mRNA, *mcherry*-mRNA, and mRNA-*luciferase*, respectively presented fluorescence/bioluminescence and on day 21, 100 % of mice expressed GFP, whereas no signal was observed for mCherry or Luciferase (Supp Fig 5).

7. Endogenous expression of ARMC2 in germ cells

Before attempting to rescue expression, we felt it was important to better characterize *Armc2* expression in healthy germ cells, and in particular to study the timing of expression.

IF was used to determine when ARMC2 protein was detectable during spermatogenesis. For these experiments, dissociated cells from testes were observed to detect the presence of ARMC2 on different spermatogenic cells. ARMC2 was present only in the flagella of the elongated spermatids (Fig 9A and Supp Fig 6A). The specificity of the signal was validated using testicular cells from Armc2 KO mice, where no signal was observed on all spermatogenic cells (Fig. 9B). In transversal sections of WT seminiferous tubules, ARMC2 signal was not present in spermatogonia and spermatocytes (Supp Fig 6B), but detected in spermatid layers.

By analyzing the RNA-seq database produced by Gan's team [28], we show that the mRNA encoding ARMC2 starts to be expressed at the pachytene spermatocyte stage, then shows a gradual increase at the round spermatid stage, and finally becomes predominantly expressed at the elongated spermatid stage (Supp Fig 6C), a result in agreement with a post-meiotic function of the protein. Finally, we also consistently observed a staining at the base of the manchette of elongating spermatids but we have no explanation for that (Fig 9A3).

In conclusion, the results presented here demonstrate that the ARMC2 protein is expressed and translated at the late stages of spermatogenesis.

8. Co-injection of *Armc2*-mRNA and *eGFP*-mRNA followed by electroporation is safe and induces green fluorescence in the seminiferous tubules.

We next tested whether the injection and electroporation of *Armc2*-mRNA molecules had any deleterious effects on testis anatomy and seminiferous tubule structure. We first verified the quality of *Armc2*-mRNA synthesis by transfecting HEK cells and performing Western blot (Supp Fig 7). After this validation, we co-injected *Armc2*-mRNA and *eGFP*-mRNA into the left testes of mice, using the right testes as untreated controls. *eGFP*-mRNA was co-injected to verify and monitor transfection efficiency. The testes were observed under a binocular microscope at different times (3-, 6-, 10-, 15-, 21-, 28- and 35-days) after electroporation to identify possible macroscopic degeneration of the seminiferous tubules. No morphological defects were observed in the testes co-injected with *Armc2*-mRNA and *eGFP*-mRNA. An example of control and injected testes from day 15 is presented in Fig 10 A1, B1. The testes were also weighed at different times post-injection, and the weight ratios of injected testes to non-injected control testes were determined. For all time points, this ratio was close to 1 (Fig 10 C), confirming that the method and the mRNAs did not cause any injury at the organ level. Next, under blue light,

595 the efficiency of the transfection was assessed by observing the GFP fluorescence at the
596 surface of the testes. GFP fluorescence was observed on testes injected with *Armc2*-mRNA
597 and *eGFP*-mRNA 2 weeks after injection (Fig 10 B2), indicating that the naked mRNA was
598 successfully transfected into testicular cells.

599 **9. Motile sperm cells detected in *Armc2* KO mice following *Armc2*-mRNA injection and**
600 **electroporation into testes**

601 We then assessed whether the injection of *Armc2*-mRNA into the testes in *Armc2* KO mice
602 restored sperm motility. We examined motility of sperm cells present in the caudal part of the
603 epididymis at different times post-injection (3- to 35-days post-injection). For each condition,
604 between 3 and 16 KO mice were used.

605 The *Armc2* KO model used is known to produce sperm cells with short and irregular flagella
606 that are therefore immotile on day 0. No motile sperm were observed on days 3, 6, 10, 15 or
607 28 after surgery (Fig 11 A). However, motile sperm cells were found in the epididymis of some
608 *Armc2* KO mice at 21- and 35-days post-treatment (Fig 11 A). Indeed, 1 in 3 mice had motile
609 sperm at 21 days post-surgery, rising to 3 in 4 mice at 35 days post-injection. Nevertheless,
610 the number of motile sperm observed remained low: 5.5 % after 21-days and 7.15 % after 35-
611 days post-injection (Fig 11 A1). The sperm motility parameters of *Armc2*$^{-/-}$-rescued motile
612 sperm were characterized in comparison to those of *Armc2*$^{+/+}$ sperm using the computer-
613 assisted semen analysis (CASA) system (Fig 11 A2). These parameters included VAP, VSL, VCL,
614 ALH, BCF, and STR. We have observed significant differences between WT and rescued sperm.
615 In particular, the VSL and LIN parameters are lower for rescued sperm. Next sperm were
616 sorted as progressive, Intermediate, hyperactivated, or slow according motility parameters of
617 motile sperm and recorded from their track (Figure 11A3).The percentage of hyperactivated
618 sperm and the proportion of intermediates in the *Armc2*$^{-/-}$-rescued motile sperm population
619 were found to be increased in comparison to the control. Videos showing sperm motility in
620 different conditions are available in the online material associated with this article (Videos 3
621 to 6).

622 After verifying motility, we looked at the morphology of the spermatozoa present in the cauda
623 epididymis. Six days after injection of *Armc2*-mRNA, the cells detected were mostly round cells
624 and abnormal spermatozoa with a short or coiled flagellum measuring between 7 and 20 µm.

The same cell types were observed at 3-, 10-, 15- and 28-days post-surgery. In contrast, the motile sperm detected on days 21 and 35, had a normal morphology with a long flagellum (greater than 100 µm) and a hook-shaped head (Fig 11 B and Supp Fig 8).

10. Motile sperm cells detected in *Armc2* KO mice following *Armc2*-mRNA injection and electroporation into testes are fertile

We subsequently evaluated the efficacy of *Armc2*-mRNA injection into the testes of *Armc2* KO mice in restoring sperm fertility. The fertility outcome was assessed through *in vitro fertilization* (IVF) and intracytoplasmic sperm injection (ICSI) experiments. The sperm rescued from *Armc2*$^{-/-}$ mice were capable of successfully fertilizing eggs and producing embryos at the two-cell stage by IVF (Fig 12 A1-A2). Notably, 62.7% of two-cell embryos were obtained with the *Armc2*$^{-/-}$-rescued sperm by IVF, compared to only 2.67% with the *Armc2*$^{-/-}$ sperm. Three % of eggs became 2-cell embryos when fertilized with sperm from *Armc2*$^{-/-}$, a rate not significantly different to that observed for eggs incubated 24 h without sperm, and likely corresponding to parthenogenesis activation (Fig 12 A1-A2).

To gain further insight, a comparative analysis of the developmental outcomes of mouse embryos generated by ICSI with spermatozoa from wild-type (WT), *Armc2*$^{-/-}$ and *Armc2*$^{-/-}$ treated mice was performed. It should be noted that in case of *Armc2*$^{-/-}$ treated mice, the ICSI procedure was performed only with the motile *Armc2*$^{-/-}$-rescue spermatozoa. The percentage of live injected oocytes that reached the blastocyst embryos was 46% for WT spermatozoa, 25% for *Armc2*$^{-/-}$-rescued spermatozoa and 13% for *Armc2*$^{-/-}$ spermatozoa (Fig. 12B). The findings indicate that the developmental potential of the embryos was enhanced when *Armc2*$^{-/-}$-rescued sperm were utilized as opposed to *Armc2*$^{-/-}$ sperm.

Overall, these results demonstrate that the *Armc2*$^{-/-}$-rescue motile spermatozoa can successfully fertilize eggs and produce embryos capable of developing properly into blastocysts.

Discussion

The challenge of treating male infertility remains to be addressed. Current assisted reproduction techniques (ARTs) are unable to treat all patients, and alternative strategies need to be developed to meet the legitimate desire to be a father. The aim of this study was to evaluate the potential of naked mRNA as a means to induce expression of exogenous

proteins in male germ cells in a preclinical adult mouse model. Based on previous studies using electroporation, we investigated whether the combination of the injection of naked mRNA and in *vivo* electroporation could lead to efficient protein expression in spermatogenic cells. We chose to first study the efficiency of capped and poly(A)-tailed mRNA coding for reporter proteins and compared results to those obtained with a non-integrative enhanced episomal vector plasmid. No EEV plasmid has ever been tested in the context of infertility treatment before this study.

Using an adult mouse model, we optimized the micro-injection and electroporation method described by Michaelis et al [15]. We show that the microinjection through the *rete testis* did not provide a homogenous distribution of the particles throughout the seminiferous tubules. Nevertheless, the seminiferous tubules remained intact, with no signal detected in the peritubular space. The peripheral expression observed was due to the close vicinity of cells to the electrodes, and to a peripheral dispersal of the injected solution, as shown by the distribution of the fluorescent i-particles NIRFiP-180. Our results also showed that the combination of injection and electroporation did not perturb spermatogenesis when electric pulses are carefully controlled. Using such a protocol, we were able to induce the expression of 3 reporter proteins, GFP, mCherry and luciferase in the testis by mRNA injection/electroporation.

Using whole testicular optical clearing, the reporter proteins were synthesized from the injected mRNA in different types of cells including Sertoli cells, spermatogonia, spermatocytes, round spermatids, and mature spermatids from day 1, and were still detectable after 1 week. These results deserve two comments: first, the expression is very fast and synthetized protein is detectable 24 h injection, second all cell types have the ability to translate mRNAs. Furthermore, the fact that we observed motile sperm at 21 days after injection confirms that spermatids are transfected and that the translation of the protein of interest is possible at this stage. For EEV, we have a similar results at day 1. However, the yields of seminiferous tubule and cellular transfection are lower. In particular, a lower level of transfection of germ cells was observed than with the mRNA. It is worth to note that after one week, the reporter proteins synthetized from injected EEV, were only discernible in the Sertoli cells.

Based on whole testes fluorescence and, for the first time, *in vivo* bioluminescence imaging of testes, we characterized the kinetics of mRNA expression. The signal measured is the fluorescence or the bioluminescence emitted by the GFP or luciferase. This signal is dependent of both the half-lives of the plasmid/mRNA and the proteins. Therefore, the kinetic of the signal persistence is a combination of the persistence of the vector and the synthetized protein. For mRNA, it's difficult to determine the lifespan of our mRNAs because these mRNAs have been modified at different levels including 5'CAP, mRNA body, poly(A)tail, which increase mRNA stability and translation [29]. Nevertheless their half-lives should not exceed few days and therefore the fluorescent signal observed, ranging from 15- to 21-days, depending on the molecule being expressed, likely corresponds to the persistence of the protein synthetized during the time window of mRNA expression. The persistence of the reporter proteins is in line with the fact that proteins involved in spermatogenesis exhibit a markedly low turnover rate [30]. This is due to the fact that these proteins are stored within sperm organelles, such as the acrosome, manchette, centrioles or fibrous sheath. These organelles, made during spermiogenesis, remain stable for weeks until the fertilization process occurs because there is no protein synthesis in mature sperm. For example, the $Ca_v3.2$ calcium channel is expressed during meiosis at the pachytene stage and contributes to calcium signaling during acrosome reaction [31-34]. When using the EEV vector, expression persisted for longer – up to 119 days – due to the intrinsec property of the EEV plasmid which allow its replication in synchronous manner with the host genome.

These results suggest that although EEV expression lasted longer, mRNAs, by targeting more efficiently male germ cells and allowing higher transfection yields of seminiferous tubules, could be a more effective and potent tool to express exogenous proteins in germ cells. By expressing a missing protein in the case of male infertility due to monogenic causes, it could be possible to restore failed spermatogenesis and thus to treat infertility.

ARMC2 is expressed in late spermatogenesis stages

We show that ARMC2 was localized in the flagellum of spermatids obtained by enzymatic dissociation. No *Armc2* expression was detected in earlier germ cell type lineages like spermatogonia or spermatocytes. These results suggest that the ARMC2 protein is expressed late during spermatogenesis, which explains why motile sperm were found in the cauda epididymis from 3-weeks after injection in our treated mice. Indeed, full spermiogenesis (from

round cell to sperm) takes around 15 days [35], and the journey across the epididymis lasts around 8 days, making a total of 3-weeks. Our results also confirm those recently published by Lechtreck et al. [36] from their study of the role of ARMC2 in the Intra-Flagellar Transport (IFT) of radial spokes in *Chlamydomonas.* They suggested that the transport of the radial spokes along the flagellum involves ARMC2, acting as an IFT adapter [36]. The presence of ARMC2 in the flagella of elongating spermatid supports this hypothesis.

Exogenous *Armc2*-mRNA expression rescued the motility of oligo-astheno-teratozoospermic sperm

This is the first demonstration that proteins can be expressed in the testis following electroporation with optimized, capped and poly(A)-tailed mRNA .

Our objective was to develop a new targeted therapeutic approach for infertility associated with monogenic defects. The objective of this preclinical study was to ascertain the efficacy of messenger RNA (mRNA) in expressing a missing protein, ARMC2, in a mouse model exhibiting oligo-astheno-teratozospermia due to the absence of *Armc2*, with the aim of restoring flagellar motility and fertility. Our results strongly suggest that the strategy did not alter spermatogenesis, as injection and electroporation of *Armc2*-mRNA or EEV-*Armc2* had no effect on testicular morphology or weight. More importantly, the technique was effective, with motile sperm cells found in cauda epididymis 3 and 5 weeks after *Armc2*-mRNA injection into testes from *Armc2* KO males. Nevertheless, it should be noted that not all injected mice were efficiently treated. For example, only 87.5% of the treated mice (14 of the 16) exhibited motile sperm after 5 weeks. The absence of motile sperm at 5 weeks may be attributed to the specific types of spermatogenic cells that were transfected during the electroporation phase. It is possible that the transfected cells may differ between individuals, potentially influenced by the injection and the position of the electrodes during electroporation. If the mRNA transfection occurs in a spermatogonia, it may take more than six weeks (including the time required to cross the epididymis) before motile epididymal sperm cells emerge. This potential timeline could explain the absence of motile sperm in some mice at 5 weeks.

Due to the quantity of motile sperm obtained, it was not possible to produce offspring through natural mating. However, the *Armc2*$^{-/-}$-rescued sperm exhibited normal morphology, motility, and *in vitro* fertility. Indeed, the *Armc2*$^{-/-}$-rescued motile spermatozoa have successfully

fertilized eggs and produced embryos that were capable of developing properly into blastocysts. These results provide compelling evidence that the method can effectively produce fertile sperm. It worth to note that the significant modifications of the CASA parameters observed for rescued sperm did not impact their fertilizing potential. Naked mRNA injection/electroporation is therefore a promising method to treat infertility. In contrast, no motile spermatozoa were found after injection/electroporation of EEV-*Armc2*, confirming our previous results suggesting that this nucleic tool does not efficiently enter or transfect germ cells.

Although this success, the transfection rate deserves to be improved to obtain a larger number of sperm cells to produced offspring through natural mating. To increase the testicular transfection rate, encapsulation of mRNA into lipids nanoparticles could be used, as used for Covid vaccination [39]. During the writing of this manuscript, Dong team [40], used a self-amplifying RNA (saRNA) encapsulated in cholesterol-amino-phosphate derived lipid nanoparticle to restore spermatogenesis in infertile mice. They successfully restore the expression of the DNA Meiotic Recombinase 1 (DMC1) [41-43] in *Dmc1* KO infertile mice by injecting a self-amplifying RNA-*Dmc1* in the testes. saRNA are genetically engineered replicons derived from self-replicating single-stranded RNA viruses [44]. The saRNA contains the alphavirus replicase genes and encodes an RNA-dependent RNA polymerase (RdRP) complex which amplifies synthetic transcripts in situ and the target RNA sequence. The target RNA is expressed at high levels as a separate entity. As a result of their self-replicative activity, saRNAs can be delivered at lower concentrations than conventional mRNA to achieve comparable expression levels [45]. Moreover, saRNA constructs need to be condensed by a cationic carrier into a nanoparticle measuring ~100 nm to enable their uptake into target cells and protect the saRNA from degradation [46]. Finally, saRNA will amplify the RNA without cellular regulation. For all these reasons, if such a strategy is to be pursued, a potential toxicity effect due to saRNA over expression must be investigated in the testes and progeny. Another difficulty with saRNA relates to the size of the molecular construct. saRNA sequences are large and complex. The length of the sequence RdRP is around 7 kilobases, which often makes the full length of saRNA more than 9 kilobases once the sequence for the protein of interest has been integrated [46]. Dong et al. [40] successfully used their saRNA construct to rescue spermatogenesis failure induced by the absence of the small protein Dmc1 (37 KDa), but it

may be more challenging with larger proteins such as the structural proteins involved in OAT, including the 98-kDa ARMC2 [23].

Our next step will be to assess whether encapsulating *Armc2*-mRNA in LNP-CAP could allow a larger number of germ cells to be transfected.

Naked mRNA, a new therapeutic strategy to treat severe infertility

Non-obstructive Azoospermia (NOA) and severe oligozoospermia (SO) are the most severe disorders of spermatogenesis and are the most likely to be of genetic origin. NOA is defined by the complete absence of spermatozoa in the ejaculate. Approximately 10–15 % of infertile men have azoospermia, and a further 15 % have SO [47]. For patients with NOA, few clinical solutions are currently available. Generally, testicular sperm extraction is attempted to collect some spermatozoa from the seminiferous tubules, which can then be used for ICSI [48]. When no sperm are retrieved, intra-conjugal conception is impossible. The results of this study strongly suggest that transient mRNA expression of a missing protein in NOA testes by electroporation could be sufficient to produce normal sperm for IVF and obtain embryos.

In conclusion, this paper presents the first *in vivo* testicular injection and electroporation of capped and poly(A)-tailed mRNA, demonstrating that it is an efficient strategy to transfect male germ cells and that the duration of expression of the resulting proteins is compatible with restoring spermatogenesis. Our comprehensive study revealed mRNA to be more efficient than an episomal vector, despite longer-lived expression in male germ cells with EEV. The difference was linked to EEV achieving a lower rate of seminiferous tubule transfection and a shorter duration of expression in germ cells. Our findings have also demonstrated, for the first time, that sperm motility and fertility can be restored in mice with an oligo-astheno-teratozoospermia phenotype through a technique that combines injection and electroporation of capped and poly(A)-tailed mRNA. The findings presented open new opportunities to develop efficient strategies to treat male infertility with monogenic causes.

804

805 **Legends**

806 **Figure 1: Distribution of I-particles NIRFIP-180 in testis injected *via* the rete testis route.**

807 (A) A solution containing 0.05 % Fast Green and 1 % fluorescent i-particles NIRFiP-180 was
808 prepared, 10 µL was injected into the seminiferous tubules of adult males, through the *rete*
809 *testes* and its efferent channels. Injection was performed at constant pressure under a
810 binocular microscope. The progression of filling of the seminiferous tubules was monitored
811 thanks to the Fast Green. (B) The testes were only filled to 2/3 capacity in order to prevent
812 damage to the tissue. (C) Representative distribution of fluorescent i-particles NIRFiP-180 in a
813 whole cross-section of an injected testis. Nuclei were counterstained with DAPI (blue
814 emission) to reveal tubules. (D) Enlargement of a seminiferous tubule showing particles
815 localized inside the lumens of the tubules. Scales bars: 1 mm and 500 µm.

816 **Figure 2: *In vivo* injection and electroporation do not alter the morphological structure of**
817 **the testes, seminiferous tubules, or sperm cells.**

818 (A, B) Testicular morphology was not affected by *in vivo* injection and electroporation of EEV-
819 *GFP* (A) or *GFP*-mRNA (B). Controls correspond to contralateral testes injected/electroporated
820 with control solution (PBS, 0.05 % FG). (A1, B1) comparison of the testicular morphology of
821 adult testes injected with nucleic acid vectors or control solutions. (A2, B2) Comparison of
822 testicular weight and (A3, B3) testicular length on day 7 after injection/electroporation. Data
823 are represented as a box plot median (n=4 for each condition). A Wilcoxon matched pairs test
824 was used to assess the significance of any differences in testis weights and lengths, and p
825 values of ≤ 0.05 were considered statistically significant. (C) Intact testicular structure after *in*
826 *vivo* injection and electroporation with EEV-*GFP* and *GFP*-mRNA. Comparison of testicular
827 cross section structures. Testes paraffin sections were stained with eosin/hematoxylin and
828 observed by light microscopy (20x magnification). (C1) Control, (C2) EEV-*GFP* injected and (C3)
829 *GFP*-mRNA injected. Scales bars: 1000 µm.

830 (D) Seminiferous tubule structures are not affected by *in vivo* injection and electroporation
831 with EEV-*GFP* and *GFP*-mRNA. Enlargement of cross sections showing the fine structure of a
832 seminiferous tubule for control (D1), EEV-*GFP* (D2) and *GFP*-mRNA (D3). In each tubule the
833 different layers of spermatogenic cells are indicated, Sertoli cells (S), Spermatogonia (Sg),

Spermatocytes (Scytes), rounds Spermatids (Stids) and sperm cells (Spz), Leydig cells (L). Scales bars: 20 µm.

(E) The area of seminiferous tubules is not affected by *in vivo* injection and electroporation with EEV-*GFP* and *GFP*-mRNA. Comparison of the seminiferous tubule diameter after injection of nucleic acid vectors or control solutions. Data are represented as a box plot median. The areas of seminiferous tubules (μm^2) were measured for round cross sections of $n > 35$ tubules per testis section (n= 5 testis sections per condition). Statistical significance was verified using a Student's *t*-test.

(F) Injection/electroporation do not impact epididymal sperm cells. Representative sperm observed by light microscopy on day 7 after injection/electroporation with Control solution (F1), EEV-*GFP* (F2), or *GFP*-mRNA (F3). Scale bars: 10 µm. (F4) Percentage of normal epididymal sperm cells in each condition. The number of males were n=5 for EEV-*GFP*; n=6 for *GFP*-mRNA and n=9 for WT. More than 150 sperm by males were analyzed. Statistical significance was verified using a one-way ANOVA test.

Figure 3: Kinetics of EEV-*GFP* expression following *in vivo* injection/electroporation: whole testicular expression

(A1-H1) Whole-mount testes on days 0, 1, 7, 14, 21, 28, 35 and 42 after *in vivo* injection/electroporation with EEV-*GFP*. (A2-H2) Under fluorescence observation, GFP expression was detectable in transfected testes from 12-week-old B6D2 mice. (C3-H3) Insets show the absence of autofluorescence in non-transfected control testes, observed under 4X magnification. The GFP expression presented a punctiform pattern in seminiferous tubules and was detected from 1 day to 42 days. Scales bars: 1 mm and 100 µm.

Figure 4: Kinetics of *GFP*-mRNA expression following *in vivo* injection/electroporation: whole testicular expression

(A1-F1) Whole-mount testes on days 0, 1, 7, 15, 21 and 28 after *in vivo* injection/ electroporation with *GFP*-mRNA. (A2-F2) Under fluorescence observation, GFP expression was detectable in transfected testes from 12-week-old B6D2 mice. (A3-F3) Insets show the absence of autofluorescence in non-transfected control testes, observed under 4X magnification.The GFP expression presented a continuous pattern in seminiferous tubules and was detected from day 1 to day 15. Scale bars: 1 mm and 100 µm.

(G) Comparison of the percentage of injected mice exhibiting reporter gene expression. Mice injected with *GFP*-mRNA exhibited GFP expression from day 1 to day 21. Mice injected with EEV-GFP exhibited GFP expression from day 1 to day 49. (for EEV-*GFP* n=11 on day 1; n=13 on day 2; n=10 on day 3; n=14 on day 7; n= 5 on day 10; n= 12 on day 15; n=11 on day 21; n= 12 on day 28; n=15 on day 35; n=17 on day 42 and n=9 on day 49) ; (for *GFP*-mRNA n=3 on day 1; n=4 on day 3; n=15 on day 7; n= 21 on day 15; n=15 on day 21 and n= 5 on day 28).

Figure 5: Kinetics of EEV and mRNA expression by *in vivo* bioluminescence imaging.

(A) *In vivo* bioluminescence imaging quantification of luciferase expression over time following injection/electroporation of EEV-*GFP-luc*. (A1) EEV-*GFP-Luc* was injected into the testes and electroporated on day 0. Bioluminescence signal was quantified at several time points. Results are expressed as the percentage of the maximal signal (mean ± SEM; n=5 mice up to D2; n=4 from D3 to D28; n=3 from D35 to D98 and n=3 from D105 to D119). (A2) *In vivo* bioluminescence images of a representative mouse at several time points after administering EEV-*GFP-LUC* or PBS, and ex vivo bioluminescence images of testes after 119 days.

(B) *In vivo* bioluminescence imaging quantification of luciferase expression over time induced by injection/electroporation of *LUC*-mRNA**.** (B1) *LUC*-mRNA was injected into the testes and electroporated on day 0. Bioluminescence signal was quantified in the whole testis at several time points. Results are expressed as the percentage of the maximal signal (mean ± SEM; n = 5 mice). (B2) *In vivo* bioluminescence images of a representative mouse at several time points after administering *LUC*-mRNA or PBS, and *ex vivo* bioluminescence images of caput, testes, and cauda after 28 days.

(C) Decay over time of the number of mice expressing reporter genes. Mice were injected on day 0 with *LUC*-mRNA or EEV-*GFP-LUC* and the number of mice showing bioluminescence in the testis was counted at different time points, from day 1 to day 119. For EEV-*GFP*: n=13 at D1; n=13 at D2; n=4 from D3 to D28; n=3 from D35 to D98 and n=3 from D105 to D119. For *LUC*-mRNA: n = 5 mice for all time points.

Figure 6: Testicular and cellular *GFP*-mRNA expression measured on optically cleared testis after 3D image reconstructions from light sheet microscopy acquisitions. Testes were injected/electroporated with *GFP*-mRNA on day 0. On day 1, whole testes were fixed and subjected to optical clearing. (A) Testes were observed before and after optical clearing on a

894 binocular microscope. The right image shows the transparency of the testis after complete
895 clearing, revealing the blue mesh throughout the organ. (B) The internal structure of a cleared
896 testis was 3D reconstructed after lightsheet microscopy image acquisition. The reconstruction
897 was possible only for a half testis due to light penetration constraints. Two opposing faces of
898 the same testis are presented, allowing the distribution of GFP fluorescence throughout the
899 seminiferous tubules to be measured. Pink fluorescence corresponds to the autofluorescence
900 of interstitial cells located around the seminiferous tubules. Scale bars A: 1 mm and B: 500
901 µm.
902
903 **Figure 7: Cellular expression of EEV-*GFP* following *in vivo* injection/ electroporation**. Testes
904 were injected/electroporated with EEV-*GFP* on day 0. On day 1 and on day 7, whole testes
905 were fixed and subjected to optical clearing. Cleared tested were observed by fluorescence
906 microscopy. (A1-A3) On day 1, transfected seminiferous tubules showed dotted green
907 fluorescence at low magnification (10x/0.45). Nuclei were counterstained with DAPI (blue
908 staining) to reveal the structure of the seminiferous tubules. At the cellular level, fluorescence
909 was detectable (B1-B3) in germ cells including Spermatogonia (Sg), Spermatocytes (Scytes)
910 and round Spermatids (RStids), as well as (C1-C3) in Sertoli cells (SC). (D1-D3) On day 7, the
911 GFP signal was lower at low magnification (10x/0.45) and detectable (E1-E3) only in Sertoli
912 cells (40x/1.15 WI) (n=3) (PTc =Peri-tubular myoid cell). E4 is an enlargement of the red square
913 in E3, allowing the cell type to be identified. Scale bars: 100 µm, 15 µm and 3 µm.

914 **Figure 8: Cellular expression of *GFP*-mRNA following *in vivo* injection/electroporation**.
915 Testes were injected/electroporated with *GFP*-mRNA on day 0. On day 1 and day 7, whole
916 testes were fixed and subjected to optical clearing. Cleared testes were observed by
917 fluorescence microscopy. (A1-A3) On day 1, transfected seminiferous tubules showed strong
918 broad-ranging green fluorescence at low magnification (10x0/0.45). Nuclei were
919 counterstained with DAPI (blue staining) to reveal the structure of the seminiferous tubule. At
920 the cellular level, fluorescence was detectable in germ cells (B1-B3) including Spermatogonia
921 (Sg), Spermatocytes (Scytes) and round Spermatids (RStids), mature spermatids cells (m-
922 Sptids) and Sertoli cells (SC). B4 is an enlargement of the red square in B3, allowing the cell
923 types to be identified. (D1-D3) On day 7, the GFP signal remained strong at low magnification
924 (10x/0.45) and was still detectable in (E1-E3) all germ cell types and Sertoli cells (40x/1.15 WI)

(n=3). E4 is an enlargement of the red square in E3, showing that testicular sperm were also stained. Scale bars: 100 µm, 15 µm and 3 µm.

Figure 9: ARMC2 localization in dissociated testicular cells observed by immunofluorescence. Cells from WT and *Armc2* KO mice were counterstained with Hoechst (A1-B1) and stained with antibodies against tubulin (A2-B2, green signal) and ARMC2 (A3-B3, red signal). (A4-B4) overlay of the different staining. In WT mice, ARMC2 is located in the flagellum of spermatids. In KO mice, no ARMC2 signal (red fluorescence) was observed in any cells.

Figure 10: *In vivo* co-injection of *Armc2*-mRNA and *eGFP*-mRNA followed by electroporation do not affect testes morphology and weight. Adult WT mouse testes were injected with a solution containing *Armc2*-mRNA and *eGFP*-mRNA. After injection, the testes were electroporated and mice were euthanized two weeks later. (A): Whole testis under white and blue lights on a fluorescence microscope (A1): control testes not injected/electroporated (A2): testes injected with *Armc2*-mRNA and *eGFP*-mRNA. *eGFP*-mRNA was co-injected to follow the transfection efficiency. (B): Ratio of injected/electroporated testis weights to control testis weights at several time points post-injection (3-, 6-, 10-, 15-, 21-, 28- and 35-days post-surgery). n= 1 mouse per time.

Figure 11: Sperm motility is restored in *Armc2* KO mice at 21 and 35 days after injection and electroporation of *Armc2*-mRNA. (A) Adult *Armc2* KO mouse testes were injected with a solution containing *Armc2*-mRNA. After injection, the testes were electroporated. At different times (3-, 6-, 10-, 15-, 21-, 28-, and 35-days *post*-injection), sperm were extracted from the cauda epididymis of the injected testis, and the sample was then examined with a CASA system to identify the percentage of motile spermatozoa (A1). n= 2 for day 15, n= 3 for days 3, 6 and 21, n= 4 for day 10, and n= 5 for days 28 and 35. (A2) Sperm motility parameters of $Armc2^{-/-}$ -rescued sperm in comparison to $Armc2^{+/+}$ sperm. The motility parameters measured were: averaged path velocity (VAP); straight line velocity (VSL); curvilinear velocity (VCL); amplitude of lateral head displacement (ALH); beat cross frequency (BCF); straightness (STR); linearity (LIN). Black dots: sperm cells from *Armc2* null mice, green dots: sperm cells from *Armc2* null mice 35 days after injection with *Armc2*-mRNA. Results are expressed as mean ± SD. (A3) Sperm motility population of $Armc2^{-/-}$ -rescued sperm in comparison to $Armc2^{-/-}$ sperm. Black column: sperm cells from *Armc2* null mice, green column: sperm cells

from *Armc2* null mice 35 days after injection with *ARmc2*-mRNA. Statistical significance was verified using a Mann-Whitney sum test. Data are displayed as mean ± SEM. P values of * ≤ 0.05, ** ≤ 0.01, or *** ≤ 0.001 were considered to represent statistically significant differences.

(B) Morphology of sperm cells in *Armc2* KO mice injected or not with *Armc2*-mRNA. (B1-B2): microscopic observation of epididymal sperm cells from a mature WT mouse. (B3-B4): epididymal sperm cells from a mature *Armc2* KO mouse 35 days after injection/electroporation with *Armc2*-mRNA. (B5-B6): epididymal sperm cells from a control *Armc2* KO male. Normal sperm cells were observed in the injected condition with *Armc2*-mRNA. (White arrow), Scale bars: 10 µm.

Fig 12: *Armc2* $^{-/-}$-rescued sperm can fertilize eggs and produce embryos by IVF and ICSI.

(A) Armc2 $^{-/-}$-rescued sperm can fertilize eggs by IVF. (A1) Illustration of 2-cell embryo obtained W/O sperm, by IVF with *Armc2*$^{-/-}$ sperm and by IVF with *Armc2*$^{-/-}$ rescued sperm; green asterisks show 2-cell embryos obtained by fertilization, red asterisks show 2-cell embryos obtained by parthenogenesis and white asterisks show unfertilized oocytes or degenerated. (A2) Histograms showing the mean percentage ± SD of alive eggs reaching the 2-cell embryo stage at 24 hours after IVF without sperm (n=4), with *Armc2*$^{-/-}$ sperm (n=4), and with *Armc2*$^{-/-}$ rescued sperm (n=5). Statistical significance was verified using a one-way ANOVA test. (B) Comparative analysis of percentage of blastocysts produced by ICSI with spermatozoa from wild-type (WT), *Armc2*$^{-/-}$ and *Armc2*$^{-/-}$-rescued individuals. For *Armc2*$^{-/-}$-rescued individuals, only motile sperm were injected. IVF and ICSI schemes were retrieved from Biorender.

Supp Fig 1: EEV and mRNA maps

(A) EEV-plasmid map. The EEV-plasmid contains GFP, EVB ori, GFP, Luciferase, and EBNA sequences under the control of the GAGs promotor. (B) The mCherry plasmid contains the mCherry gene under the control of a T7 promotor. (C) The EEV-*Armc2* plasmid contains GFP, oriP, EBNA and *Armc2* sequences under the control of the CMV and T7 promotors. (D) *mcherry*-mRNA was synthetized as described in Material and Methods. It was validated by agarose gel electrophoresis: Lane 1: DNA size marker ladder (100 bp), lane 2: capped *mcherry*-mRNA (IVT product), lane 3: *mcherry*-mRNA after DNAse treatment. Capped and poly A tailed *mcherry*-mRNA migrated to the expected size of 876 bp.

Supp Fig 2: Damaged tubules observed by optical microscopy following overstimulation

Adult mouse testes were *in vivo* injected and over electroporated using 10 square electric pulses to induce damage. (A) Control testis (no injection/electroporation). (B1-B2) Over electroporated testes showing damaged tubules as pearly white striations. Scale bars: 1 mm.

Supp Fig 3: Testicular expression of *mcherry*-mRNA following in vivo electroporation

(A1, B1, C1, D1, E1 and F1) Whole-mount testes on days 0, 1, 7, 14, 21, 28 after *in vivo* injection/ electroporation. (A2, B2, C2, D2, E2 and, F2) Using fluorescence microscopy, transfected testes from 12-week-old B6D2 mice express red mCherry fluorescence. mCherry was detected in a diffuse pattern throughout the seminiferous tubules from day 1 to day 15. (A3, B3, C3, D3, E3 and F3) images showing the absence of autofluorescence in non-transfected control testes observed at 4x magnification. Scales bars: 1 mm and 100 µm.

Supp Fig 4: Cellular expression of *mcherry*-mRNA following in vivo injection/ electroporation.

Cross sections (20 µm) of mouse testes on day 1 (AB) and day 7 (CD) after in vivo injection and electroporation with *mcherry*-mRNA, observed under fluorescence microscopy. Red signals correspond to successfully transfected testicular tubular cells; nuclei were counterstained with DAPI (blue). At the cellular level, mCherry fluorescence was detectable in Sertoli cells (SC); Spermatogonia (SG); Spermatocytes (Scytes); round Spermatids (RStids), and mature spermatids (m-Sptids) ; Scale bars: 10 µm and 5 µm.

Supp Fig 5: Decay over time of the number of mice exhibiting reporter gene expression following injection/electroporation of the three different mRNAs.

Mice were injected on day 0 with *LUC*-mRNA, *GFP*-mRNA or *mcherry*-mRNA and the number of mice showing bioluminescence or fluorescence in the testis was counted at different time points. For *LUC*-mRNA n= 5 mice at each time point. For *mcherry*-mRNA n=3 on day 1; n=4 on day3; n=15 on day 7; n= 21 on day 15; n=15 on day 21; n= 5 on day 28; n=5 on day 35; and for *GFP*-mRNA n=3 on day 12; n=7 on day 2; n=7 on day 3; n=12 on day 7; n= 13 on day 15; n=10 on day 21 ; n= 9 on day 28; n=17 on day 35 and n=5 on day 42.

Supp Fig 6: *Armc2* expression and localization in mice testis

(A) IF experiment on dissociated spermatogenic cell from WT male. (A1) Nuclei were counterstained with DAPI (blue staining), (A2) tubulin (green signal) and (A3) ARMC2 (red

signal). (A4) overlay. ARMC2 is located in the flagellum of spermatids Scale bars: 5 µm. (B) Cross-sections of seminiferous tubules (B1) Nuclei were counterstained with DAPI (blue staining), (B2) and (B2) ARMC2 (red signal). (B3) overlay. B4 is an enlargement of the red square in B3, showing that only elongating/mature spermatids were stained. (C) Expression of *Armc2* in mouse spermatogenic cells based on the RNA-sequencing study from Gan et al. 2013. Primitive type A spermatogonia (priSG-A) were isolated from 6 dpp mice; Type A spermatogonia (SG-A) and type B spermatogonia (SG-B) were from 8 dpp mice; preleptotene spermatocytes (plpSC) and pachytene spermatocytes (pacSC) were from 17 dpp mice; and round spermatids (rST), elongating spermatids (eST) and spermatozoa (SZ) were from 60 dpp mice. Artificial units (AU). Dpp: day post partum

Supp Fig 7: Validation of *Armc2*-mRNA in HEK cells.

HEK cells were transfected with *Armc2*-mRNA or EEV-*Armc2.* ARMC2 protein was detected by Western blot with an anti-HA primary antibody. The expected size for the ARMC2 protein is 98 kDa**.**

Supp Fig 8: Morphology of sperm cells from WT, *Armc2* KO and *Armc2*-rescued males.

Microscopic observation of epididymal sperm cells from WT, *Armc2* KO and *Armc2* KO-*Armc2*-mRNA injected males at 20x (left column), 40x (middle column) and 100x (right column) magnifications. In the rescue condition, rescued sperm cells were labelled with a white asterisk. Scale bars: 100, 50 and 10 µm.

Videos 1 and 2: 3D-microscopic reconstructions of face 1 and 2 of a testis injected with *GFP*-mRNA.

Video 3: CASA recording of WT epididymal sperm cells

Video 4: CASA recording of *Armc2* KO epididymal sperm cells

Videos 5 and 6: CASA recordings of epididymal sperm cells from *Armc2* KO mice on day 21 and day 35, respectively, after injection/electroporation with *Armc2*-mRNA.

Acknowledgments

This work was supported by CNRS, INSERM and ANR-20-CE18-0007 grant to JE. This work was supported by the Fondation pour la Recherche Médicale, grant number « ECO202006011669 » to CV.

Bibliography

1. Boivin, J., et al., *International estimates of infertility prevalence and treatment-seeking: potential need and demand for infertility medical care.* Hum Reprod, 2007. **22**(6): p. 1506-12.
2. Thonneau, P. and A. Spira, *Prevalence of infertility: international data and problems of measurement.* Eur J Obstet Gynecol Reprod Biol, 1991. **38**(1): p. 43-52.
3. Kekalainen, J., *Genetic incompatibility of the reproductive partners: an evolutionary perspective on infertility.* Hum Reprod, 2021. **36**(12): p. 3028-3035.
4. Kumar, N. and A.K. Singh, *Trends of male factor infertility, an important cause of infertility: A review of literature.* J Hum Reprod Sci, 2015. **8**(4): p. 191-6.
5. Uhlen, M., et al., *Transcriptomics resources of human tissues and organs.* Mol Syst Biol, 2016. **12**(4): p. 862.
6. Thonneau, P., et al., *Incidence and main causes of infertility in a resident population (1,850,000) of three French regions (1988-1989).* Hum Reprod, 1991. **6**(6): p. 811-6.
7. Cavallini, G., *Male idiopathic oligoasthenoteratozoospermia.* Asian J Androl, 2006. **8**(2): p. 143-57.
8. Colpi, G.M., et al., *European Academy of Andrology guideline Management of oligo-asthenoteratozoospermia.* Andrology, 2018. **6**(4): p. 513-524.
9. Hansen, M., et al., *Assisted reproductive technologies and the risk of birth defects--a systematic review.* Hum Reprod, 2005. **20**(2): p. 328-38.
10. Halliday, J.L., et al., *Increased risk of blastogenesis birth defects, arising in the first 4 weeks of pregnancy, after assisted reproductive technologies.* Hum Reprod, 2010. **25**(1): p. 59-65.
11. Davies, M.J., et al., *Reproductive technologies and the risk of birth defects.* N Engl J Med, 2012. **366**(19): p. 1803-13.
12. Kurinczuk, J.J., M. Hansen, and C. Bower, *The risk of birth defects in children born after assisted reproductive technologies.* Curr Opin Obstet Gynecol, 2004. **16**(3): p. 201-9.
13. Usmani, A., et al., *A non-surgical approach for male germ cell mediated gene transmission through transgenesis.* Sci Rep, 2013. **3**: p. 3430.
14. Raina, A., et al., *Testis mediated gene transfer: in vitro transfection in goat testis by electroporation.* Gene, 2015. **554**(1): p. 96-100.
15. Michaelis, M., A. Sobczak, and J.M. Weitzel, *In vivo microinjection and electroporation of mouse testis.* J Vis Exp, 2014(90).
16. Wang, L., et al., *Testis electroporation coupled with autophagy inhibitor to treat non-obstructive azoospermia.* Mol Ther Nucleic Acids, 2022. **30**: p. 451-464.
17. Duan, D., *Full-length dystrophin gene therapy for Duchenne muscular dystrophy.* Mol Ther, 2024. **32**(9): p. 2817-2818.
18. Jacobson, S.G., et al., *Safety and improved efficacy signals following gene therapy in childhood blindness caused by GUCY2D mutations.* iScience, 2021. **24**(5): p. 102409.
19. Liu, S., *Legal reflections on the case of genome-edited babies.* Glob Health Res Policy, 2020. **5**: p. 24.
20. Sadelain, M., E.P. Papapetrou, and F.D. Bushman, *Safe harbours for the integration of new DNA in the human genome.* Nat Rev Cancer, 2011. **12**(1): p. 51-8.
21. Ishii, T., *Germ line genome editing in clinics: the approaches, objectives and global society.* Brief Funct Genomics, 2017. **16**(1): p. 46-56.
22. Parhiz, H., E.N. Atochina-Vasserman, and D. Weissman, *mRNA-based therapeutics: looking beyond COVID-19 vaccines.* Lancet, 2024. **403**(10432): p. 1192-1204.

23. Coutton, C., et al., *Bi-allelic Mutations in ARMC2 Lead to Severe Astheno-Teratozoospermia Due to Sperm Flagellum Malformations in Humans and Mice.* Am J Hum Genet, 2019. **104**(2): p. 331-340.
24. in *Transforming and Scaling Up Health Professionals' Education and Training: World Health Organization Guidelines 2013*. 2013: Geneva.
25. Yoshida, N. and A.C. Perry, *Piezo-actuated mouse intracytoplasmic sperm injection (ICSI).* Nat.Protoc., 2007. **2**(2): p. 296-304.
26. Ruthig, V.A. and D.J. Lamb, *Updates in Sertoli Cell-Mediated Signaling During Spermatogenesis and Advances in Restoring Sertoli Cell Function.* Front Endocrinol (Lausanne), 2022. **13**: p. 897196.
27. de Boer, P., M. de Vries, and L. Ramos, *A mutation study of sperm head shape and motility in the mouse: lessons for the clinic.* Andrology, 2015. **3**(2): p. 174-202.
28. Gan, H., et al., *Dynamics of 5-hydroxymethylcytosine during mouse spermatogenesis.* Nat Commun, 2013. **4**: p. 1995.
29. Liu, A. and X. Wang, *The Pivotal Role of Chemical Modifications in mRNA Therapeutics.* Front Cell Dev Biol, 2022. **10**: p. 901510.
30. Hermann, B.P., et al., *The Mammalian Spermatogenesis Single-Cell Transcriptome, from Spermatogonial Stem Cells to Spermatids.* Cell Rep, 2018. **25**(6): p. 1650-1667 e8.
31. Arnoult, C., et al., *Control of the low voltage-activated calcium channel of mouse sperm by egg ZP3 and by membrane hyperpolarization during capacitation.* Proc Natl Acad Sci U S A, 1999. **96**(12): p. 6757-62.
32. Escoffier, J., et al., *Expression, localization and functions in acrosome reaction and sperm motility of Ca(V)3.1 and Ca(V)3.2 channels in sperm cells: an evaluation from Ca(V)3.1 and Ca(V)3.2 deficient mice.* J Cell Physiol, 2007. **212**(3): p. 753-63.
33. Saunders, C.M., et al., *PLC zeta: a sperm-specific trigger of Ca(2+) oscillations in eggs and embryo development.* Development, 2002. **129**(15): p. 3533-44.
34. Saunders, C.M., K. Swann, and F.A. Lai, *PLCzeta, a sperm-specific PLC and its potential role in fertilization.* Biochem Soc Symp, 2007(74): p. 23-36.
35. Ibtisham, F., et al., *Progress and future prospect of in vitro spermatogenesis.* Oncotarget, 2017. **8**(39): p. 66709-66727.
36. Lechtreck, K.F., et al., *Chlamydomonas ARMC2/PF27 is an obligate cargo adapter for intraflagellar transport of radial spokes.* Elife, 2022. **11**.
37. Kubo, T., et al., *Together, the IFT81 and IFT74 N-termini form the main module for intraflagellar transport of tubulin.* J Cell Sci, 2016. **129**(10): p. 2106-19.
38. Dai, J., et al., *In vivo analysis of outer arm dynein transport reveals cargo-specific intraflagellar transport properties.* Mol Biol Cell, 2018. **29**(21): p. 2553-2565.
39. Schoenmaker, L., et al., *mRNA-lipid nanoparticle COVID-19 vaccines: Structure and stability.* Int J Pharm, 2021. **601**: p. 120586.
40. Du, S., et al., *Cholesterol-Amino-Phosphate (CAP) Derived Lipid Nanoparticles for Delivery of Self-Amplifying RNA and Restoration of Spermatogenesis in Infertile Mice.* Adv Sci (Weinh), 2023. **10**(11): p. e2300188.
41. Takemoto, K., et al., *Meiosis-Specific C19orf57/4930432K21Rik/BRME1 Modulates Localization of RAD51 and DMC1 to DSBs in Mouse Meiotic Recombination.* Cell Rep, 2020. **31**(8): p. 107686.
42. Habu, T., et al., *The mouse and human homologs of DMC1, the yeast meiosis-specific homologous recombination gene, have a common unique form of exon-skipped transcript in meiosis.* Nucleic Acids Res, 1996. **24**(3): p. 470-7.
43. Shinohara, A., et al., *Saccharomyces cerevisiae recA homologues RAD51 and DMC1 have both distinct and overlapping roles in meiotic recombination.* Genes Cells, 1997. **2**(10): p. 615-29.
44. Tews, B.A. and G. Meyers, *Self-Replicating RNA.* Methods Mol Biol, 2017. **1499**: p. 15-35.
45. Bloom, K., F. van den Berg, and P. Arbuthnot, *Self-amplifying RNA vaccines for infectious diseases.* Gene Ther, 2021. **28**(3-4): p. 117-129.
46. Kim, J., et al., *Self-assembled mRNA vaccines.* Adv Drug Deliv Rev, 2021. **170**: p. 83-112.

47. Cocuzza, M., C. Alvarenga, and R. Pagani, *The epidemiology and etiology of azoospermia.* Clinics (Sao Paulo), 2013. **68 Suppl 1**: p. 15-26.
48. Ma, Y., et al., *A risk prediction model of sperm retrieval failure with fine needle aspiration in males with non-obstructive azoospermia.* Hum Reprod, 2019. **34**(2): p. 200-208.

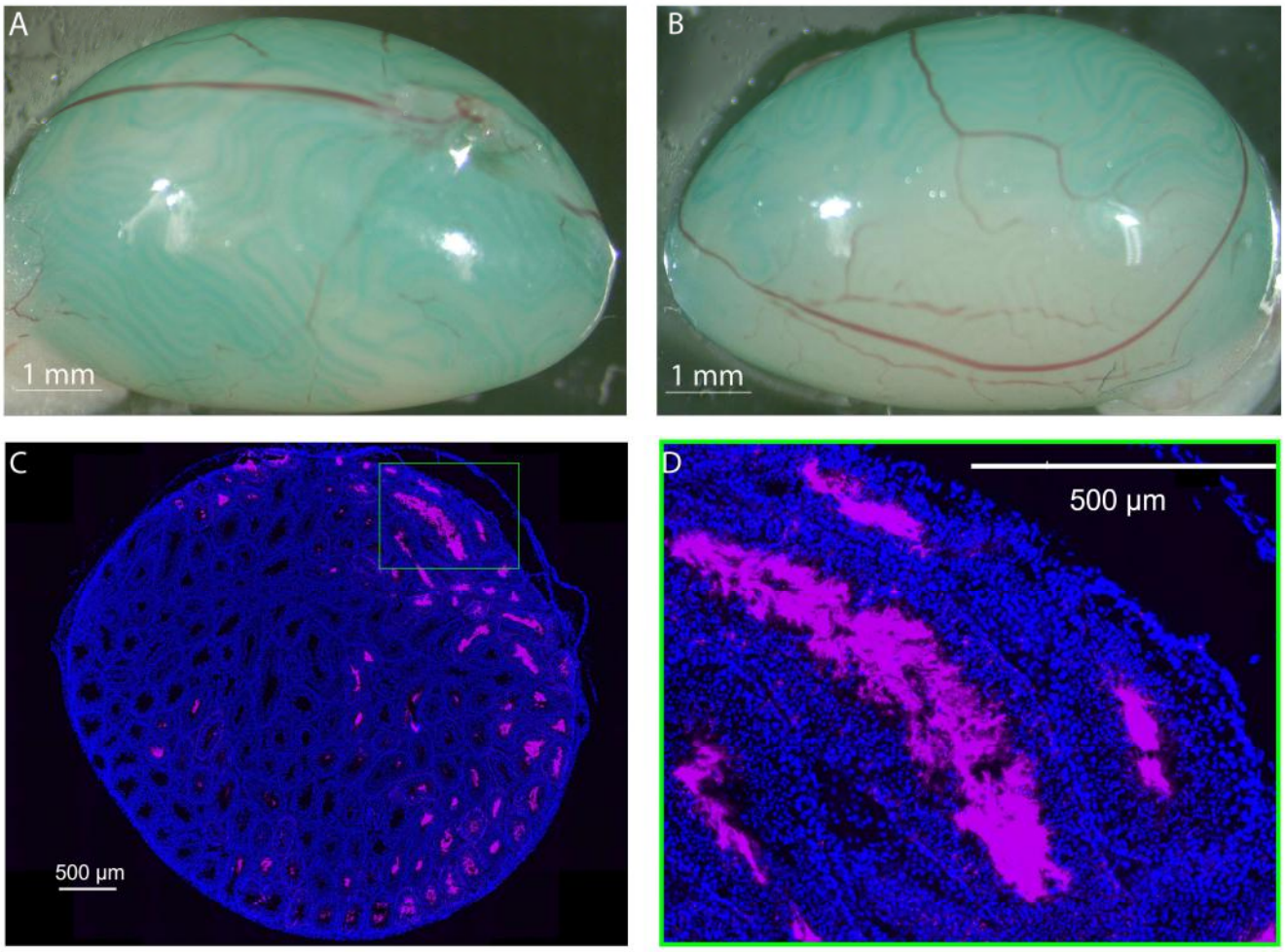

Figure 1, Vilpreux et al 2023

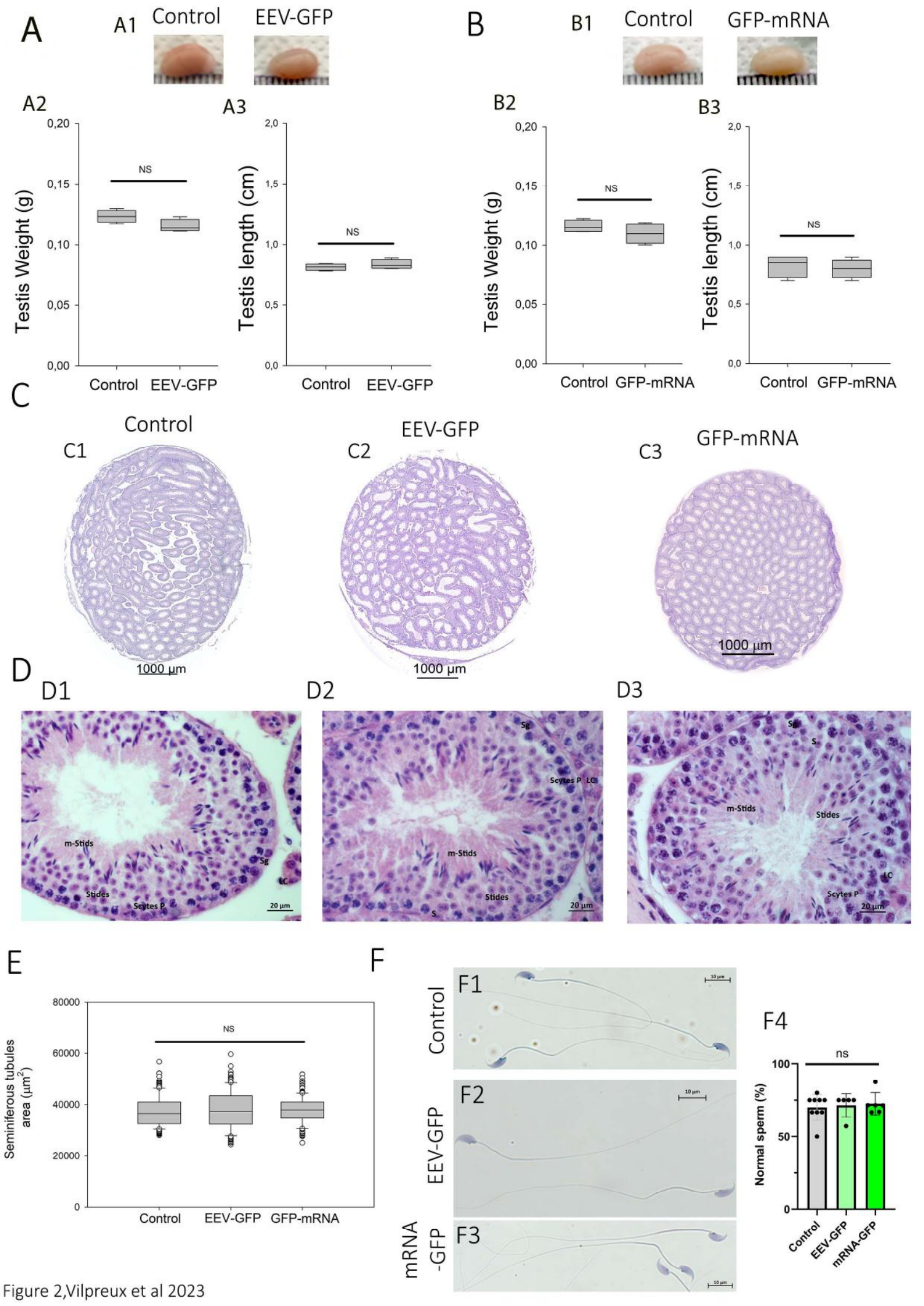

Figure 2,Vilpreux et al 2023

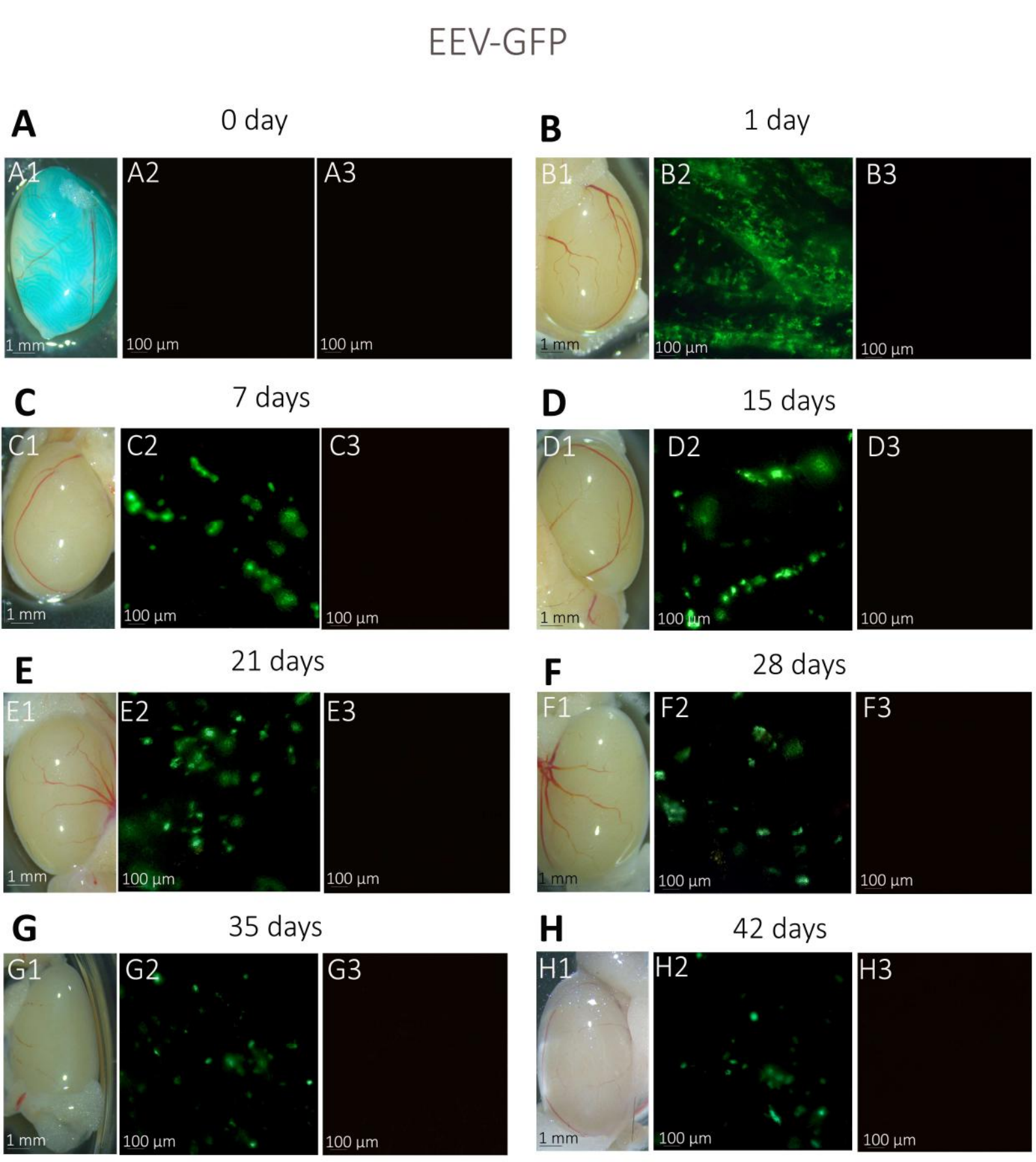

Figure 3,Vilpreux et al 2023

GFP-mRNA

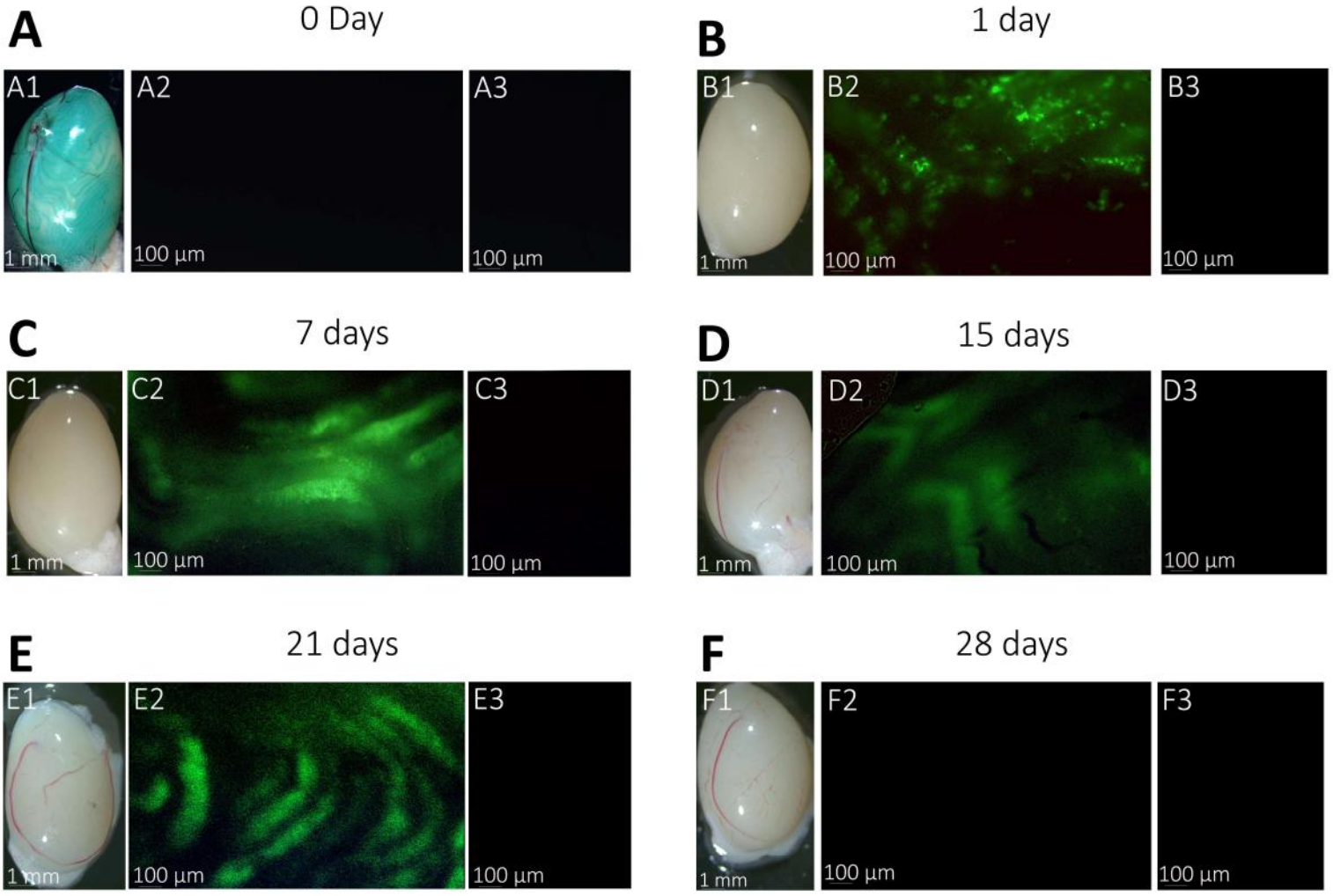

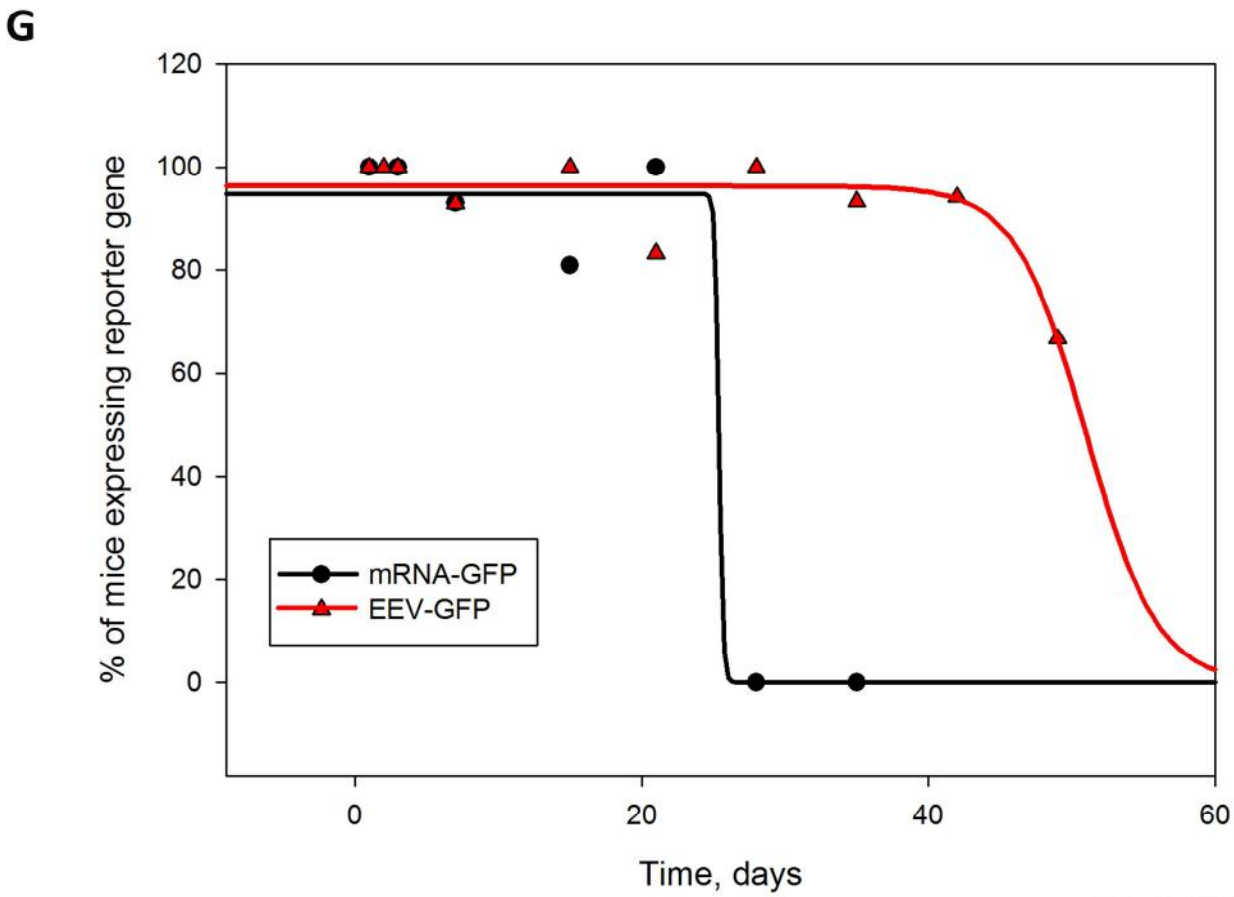

Fig4, Vilpreux et al 2023

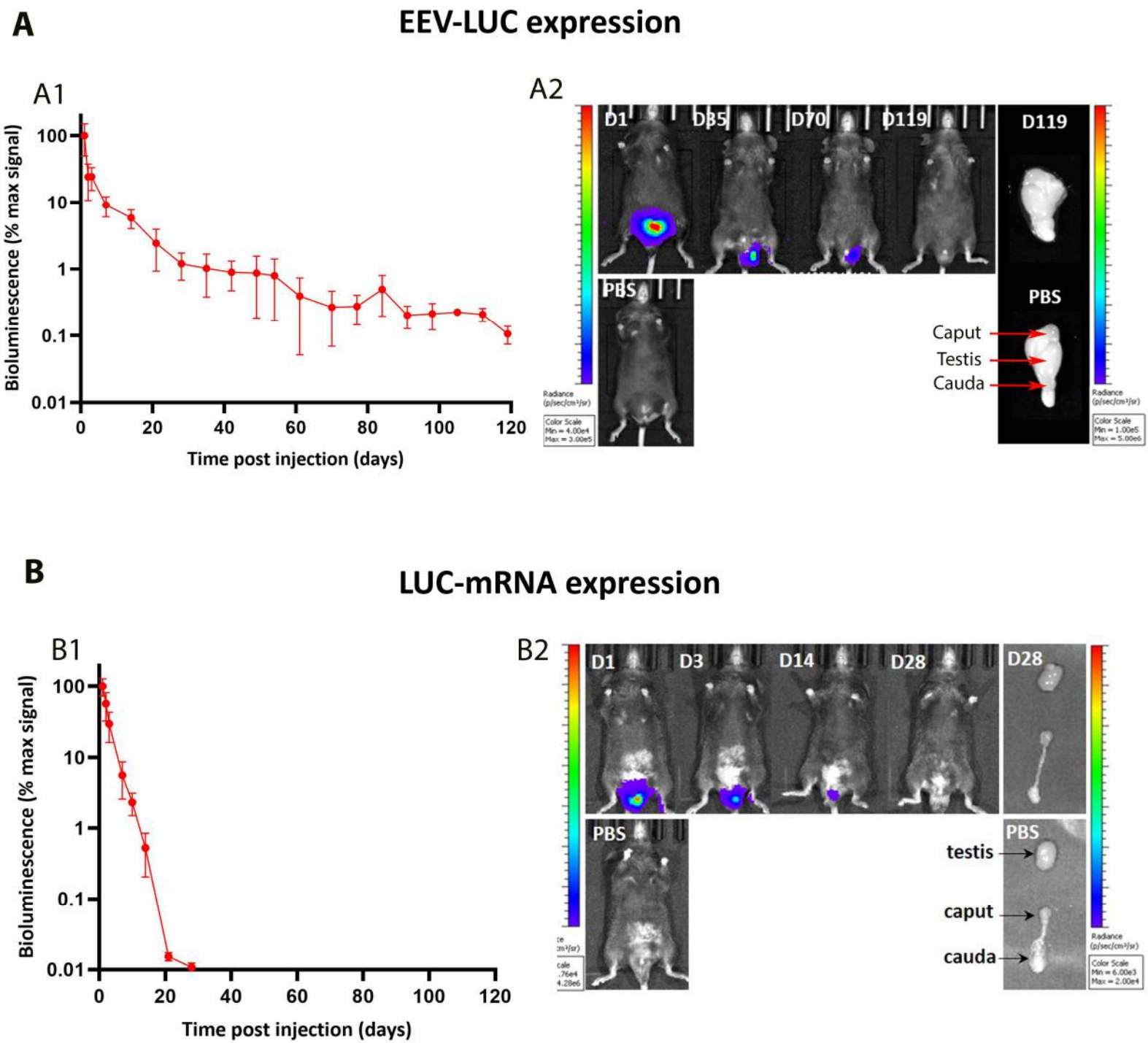

Figure 5, Vilpreux et al 2023

GFP-mRNA 1 day post injection

A

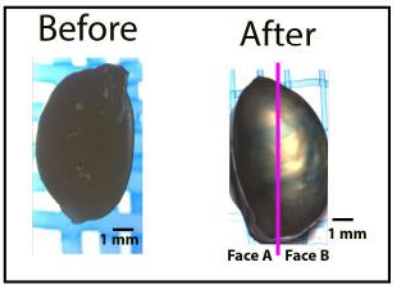

B

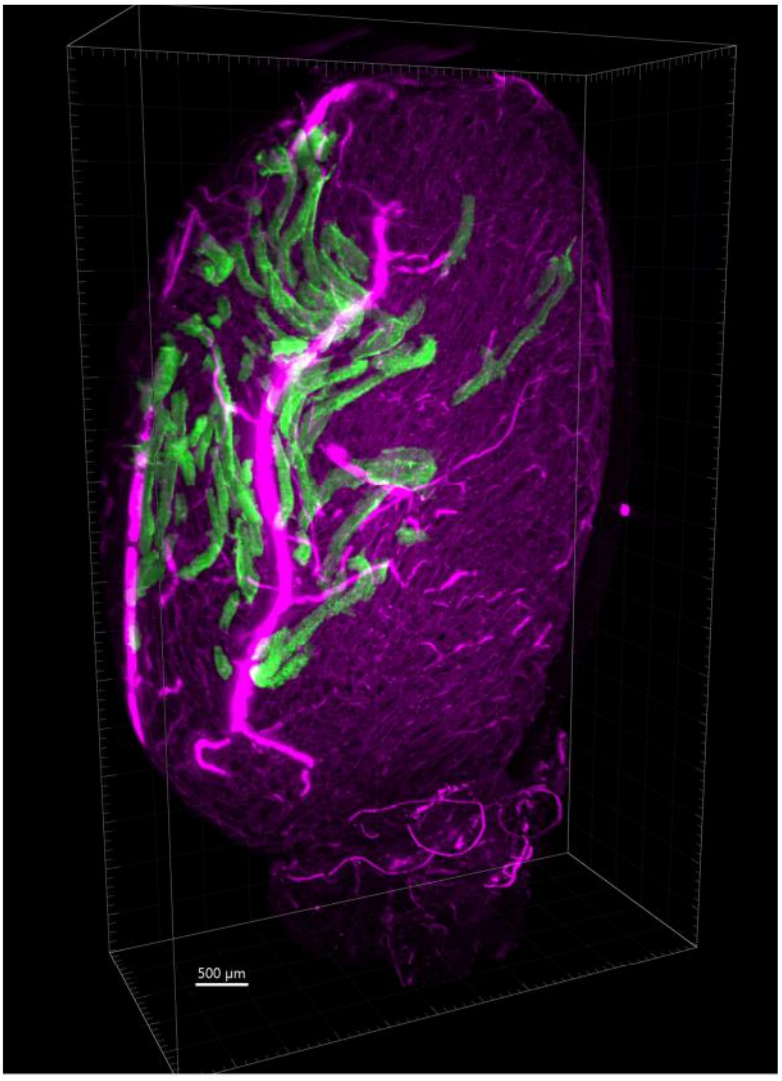

Face A

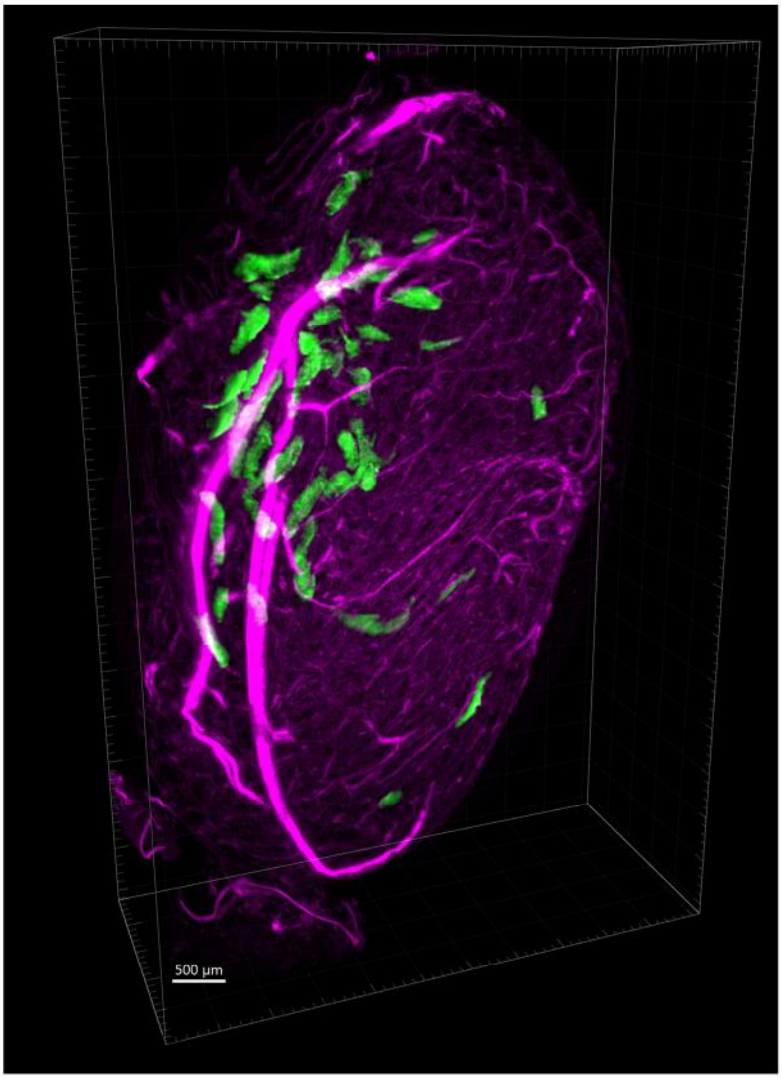

Face B

Figure 6, Vilpreux et al 2023

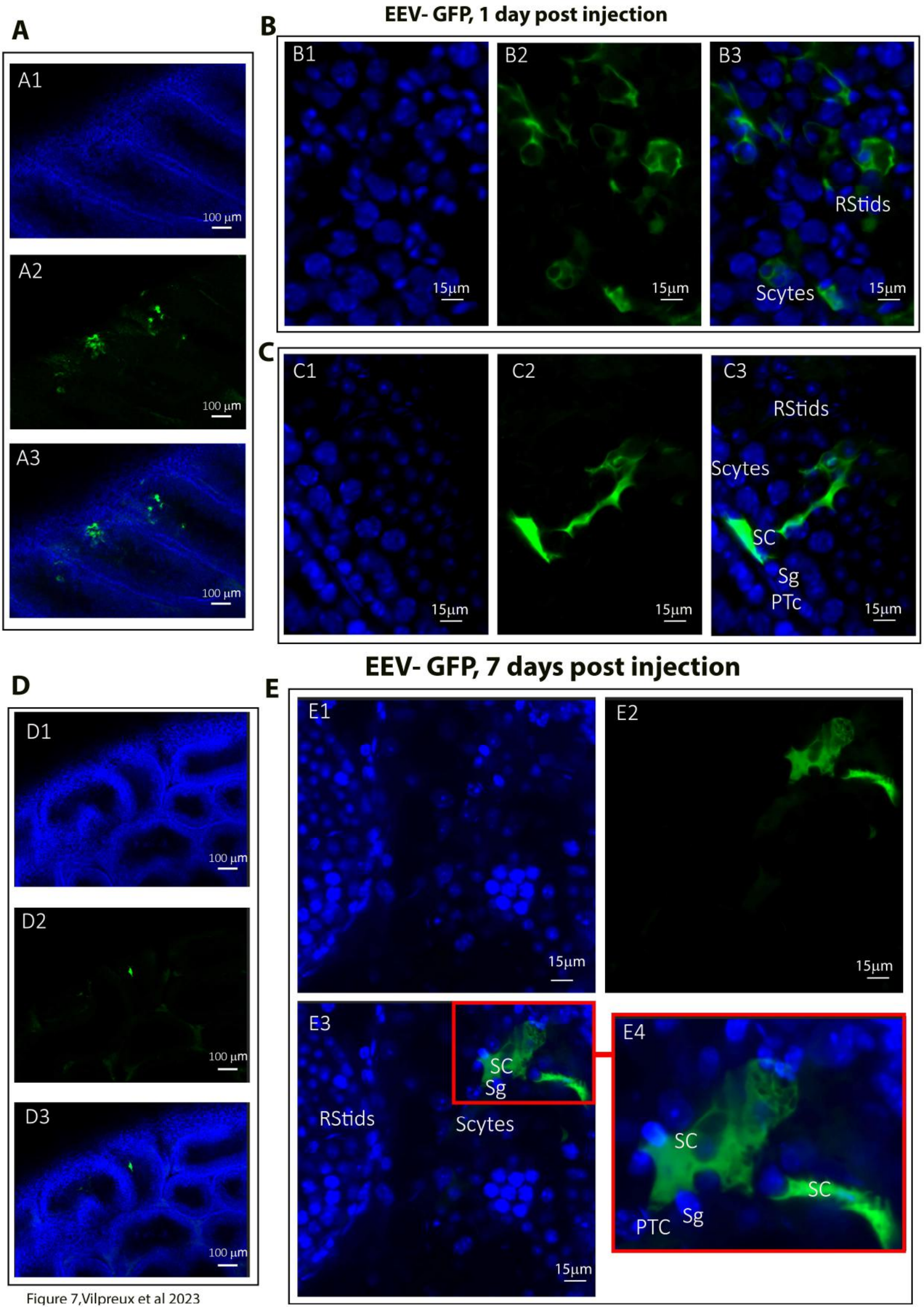

Figure 7,Vilpreux et al 2023

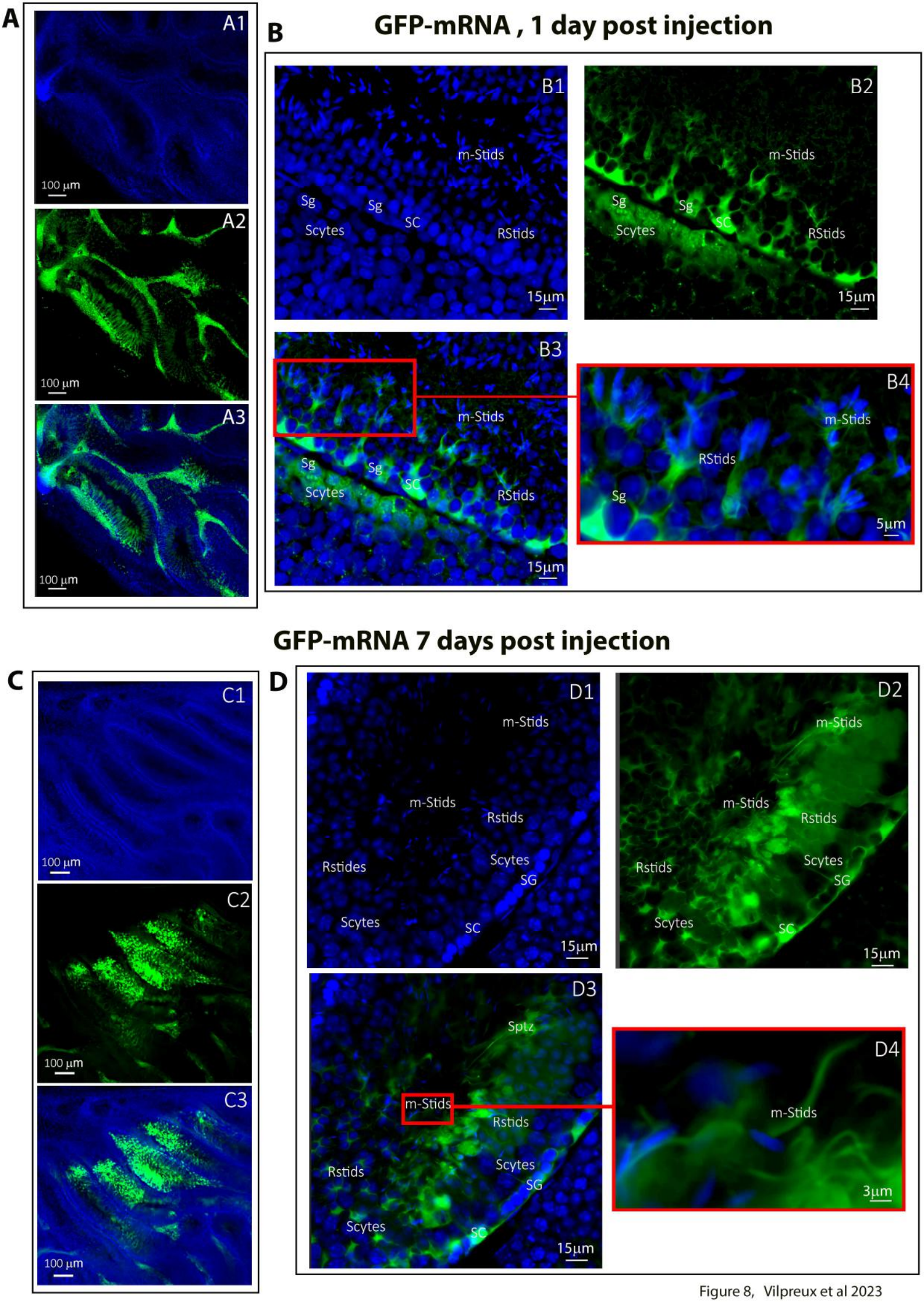

Figure 8, Vilpreux et al 2023

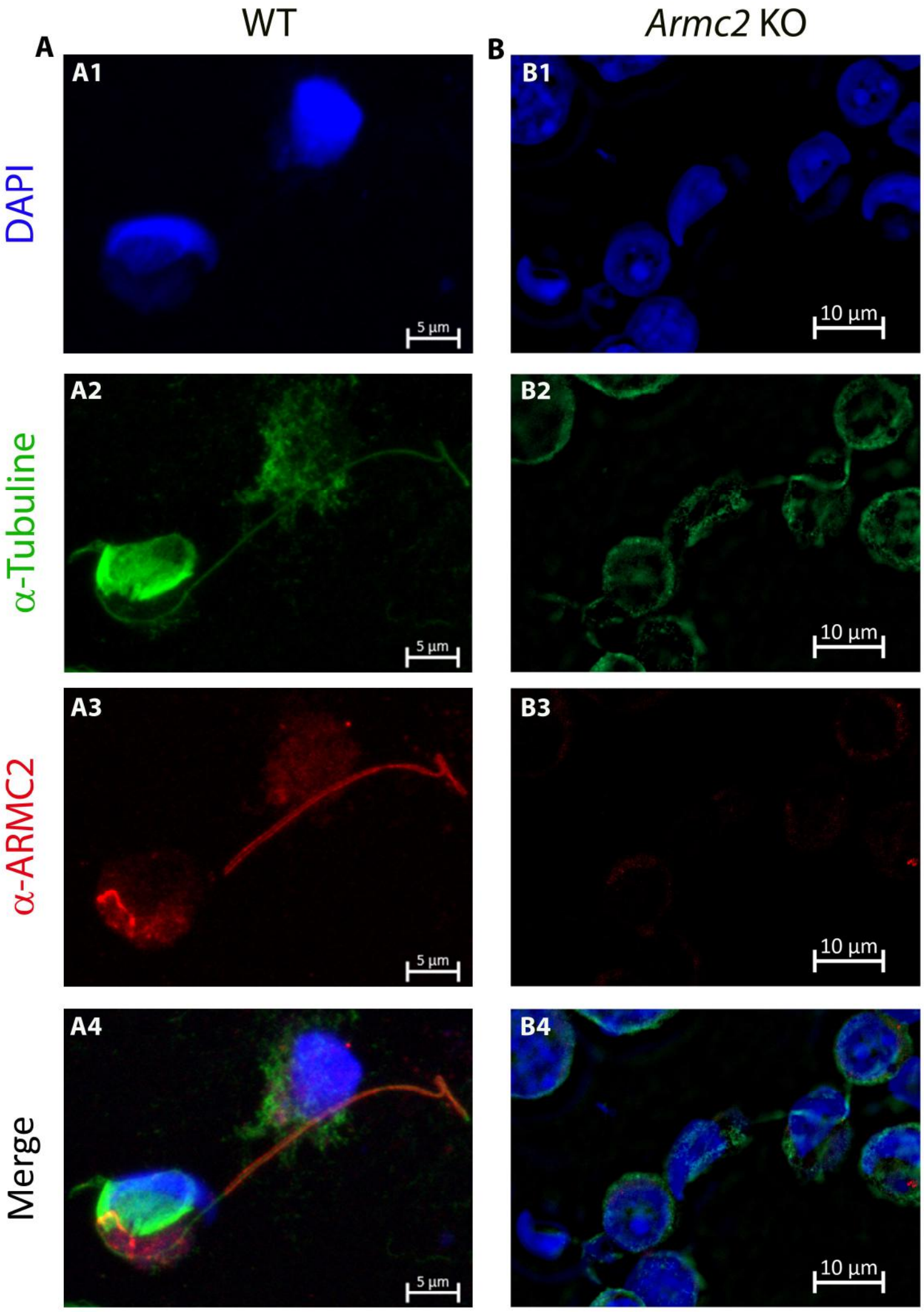

Figure 9, Vilpreux et al 2023

A

Control, 7 day post injection

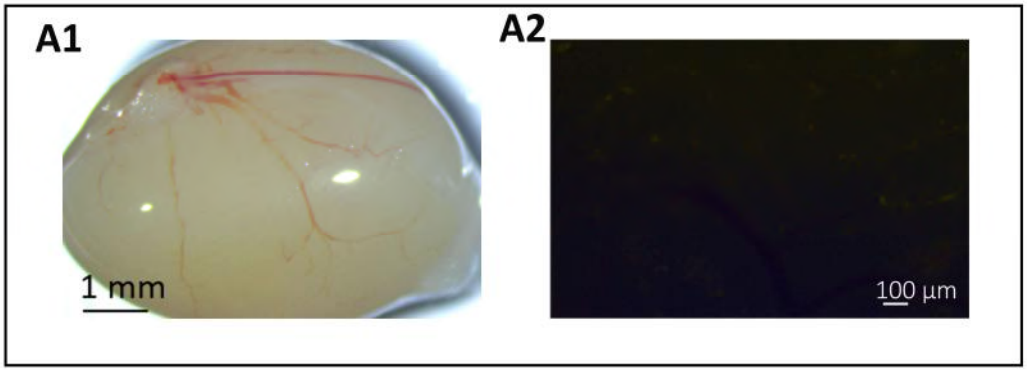

B

Armc2-mRNA + eGFP-mRNA, 7 day post injection

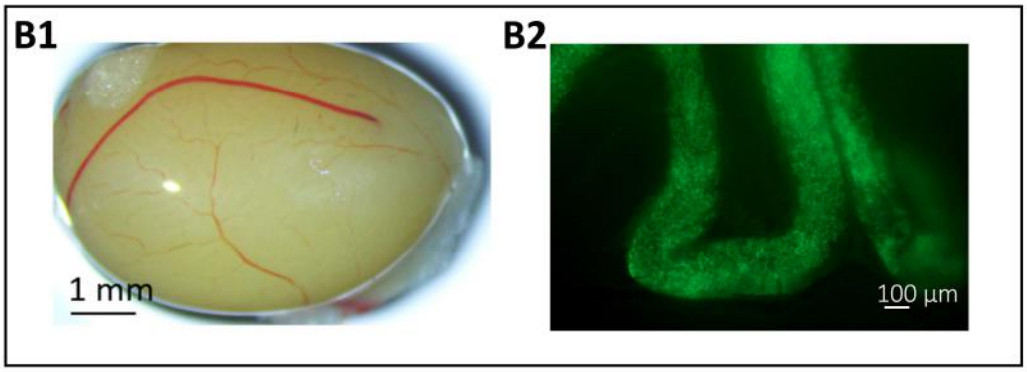

C

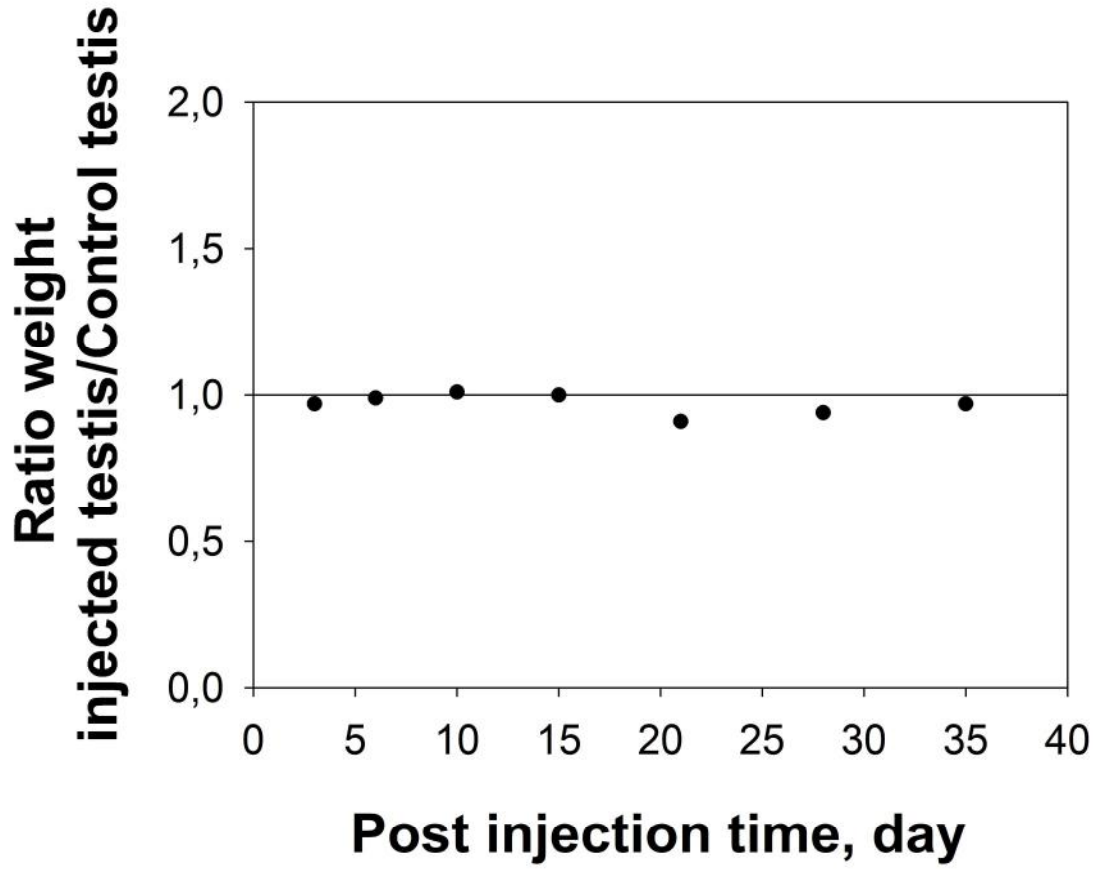

Figure 10, Vilpreux et al 2023

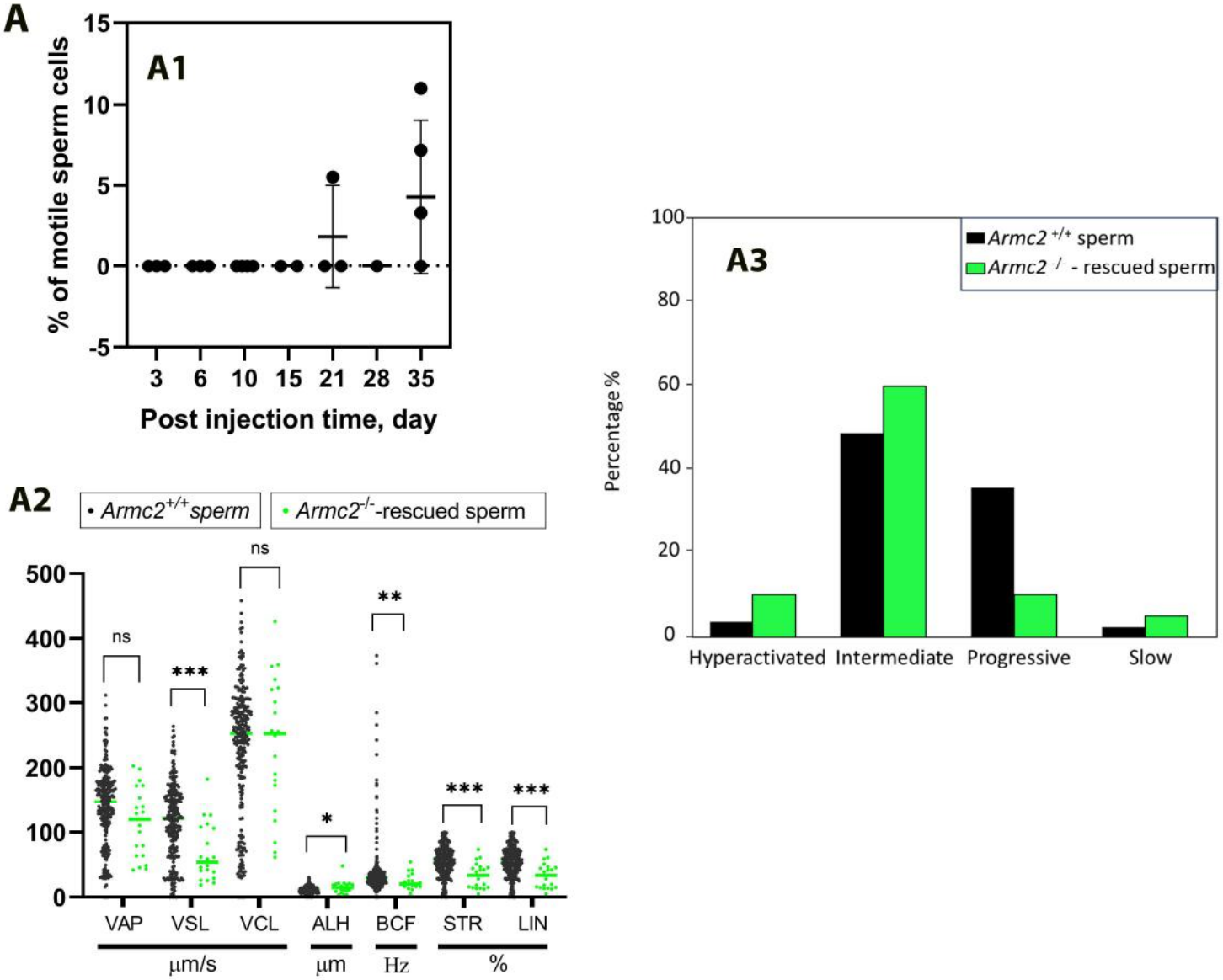

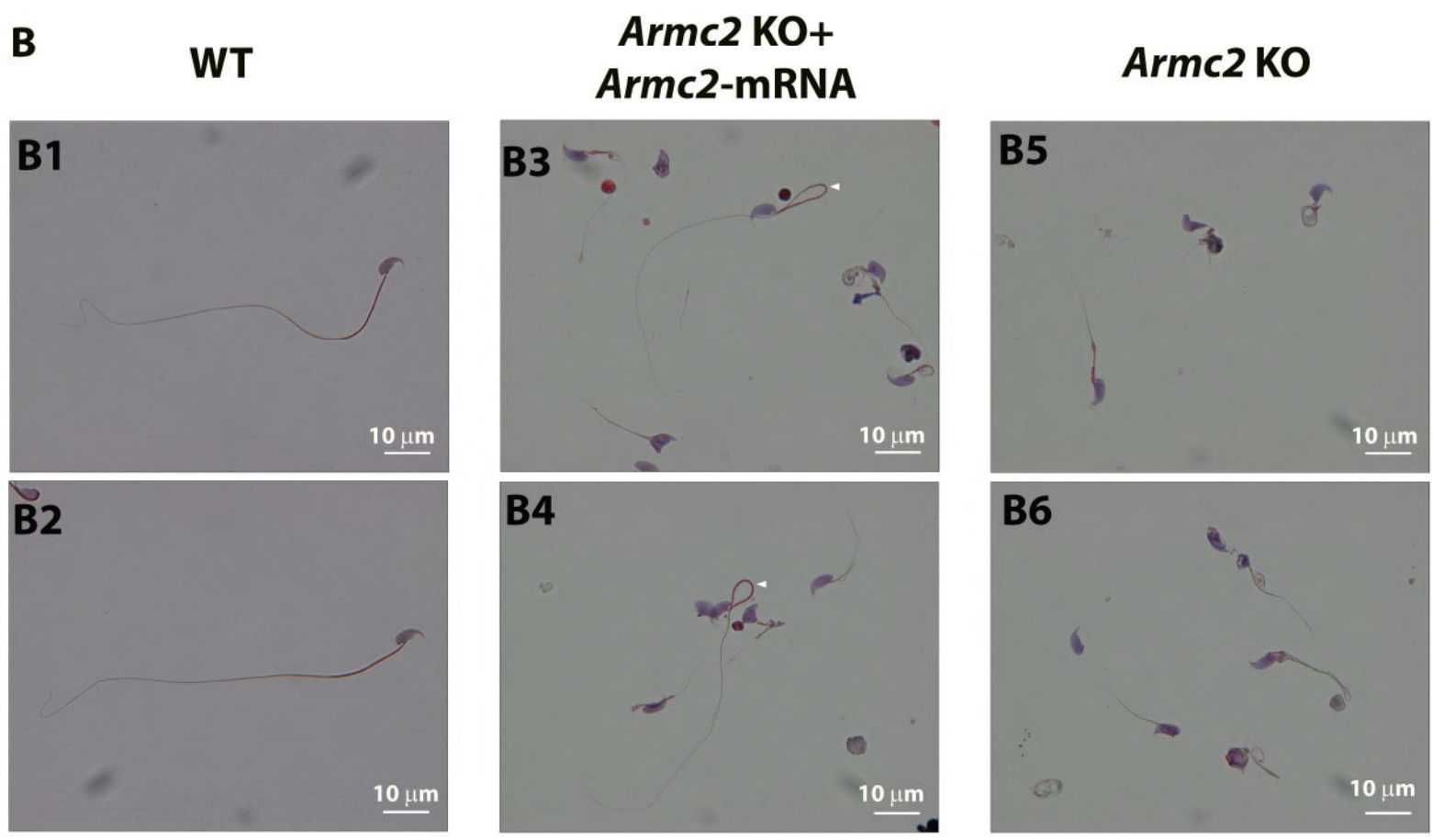

Figure 11,Vilpreux et al 2023

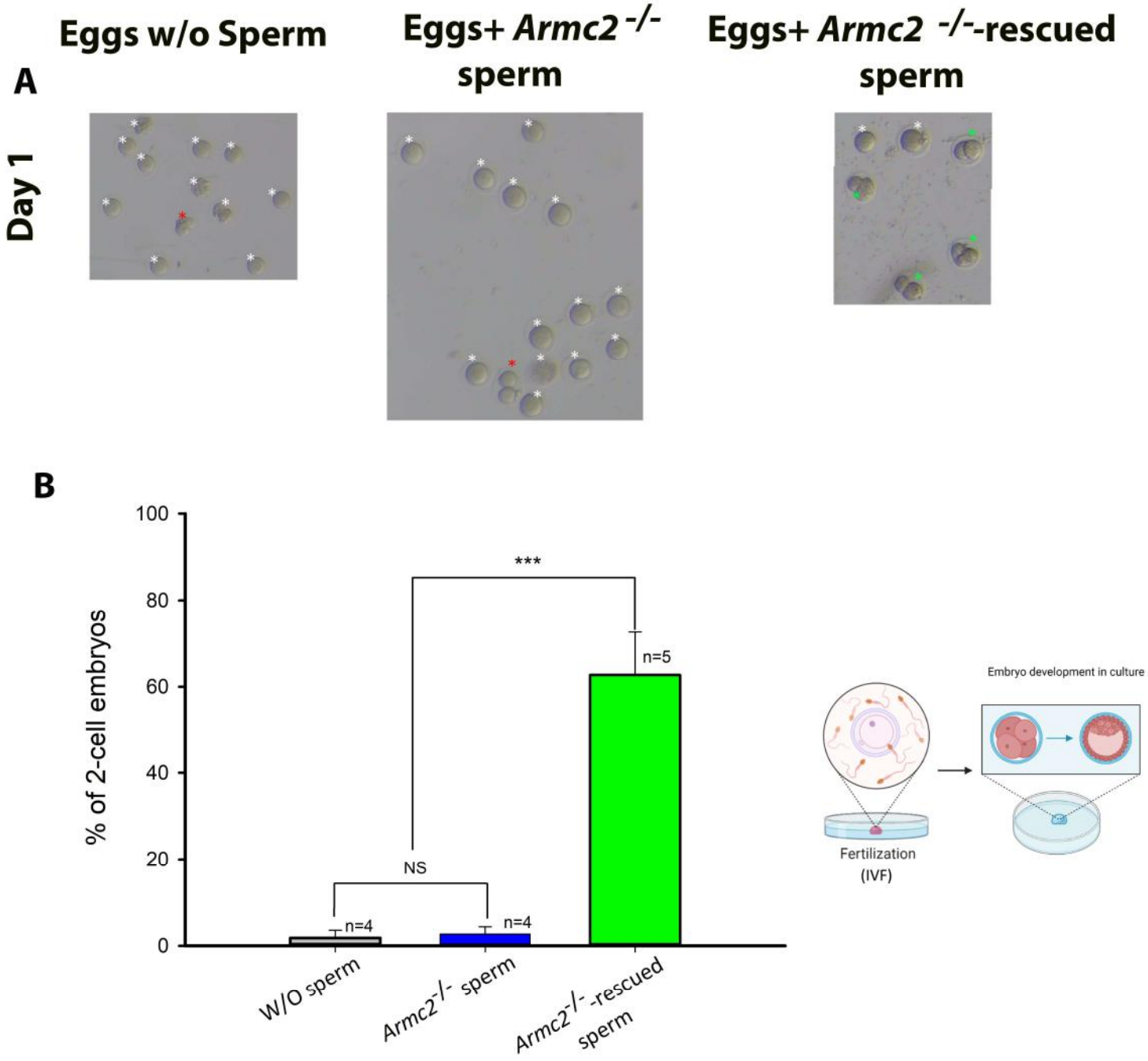

Figure 12, Vilpreux et al 2023

A

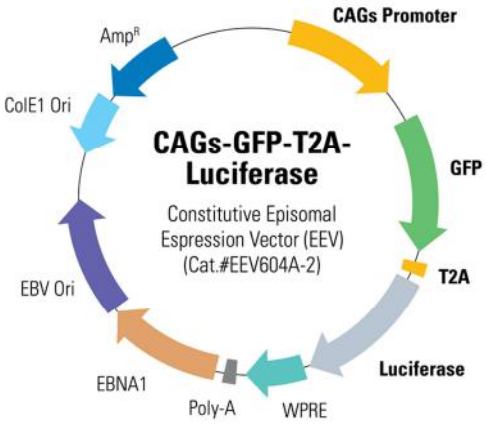

B

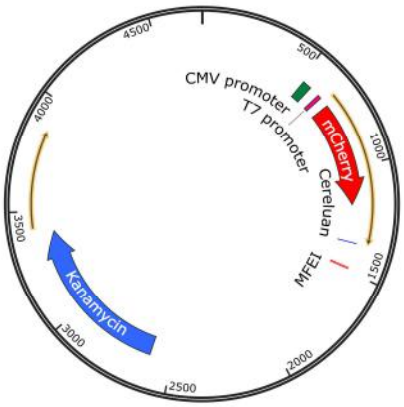

C

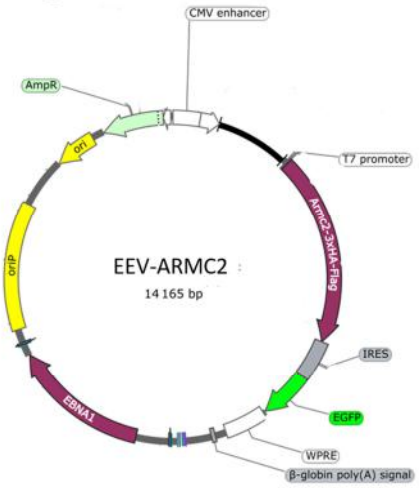

D

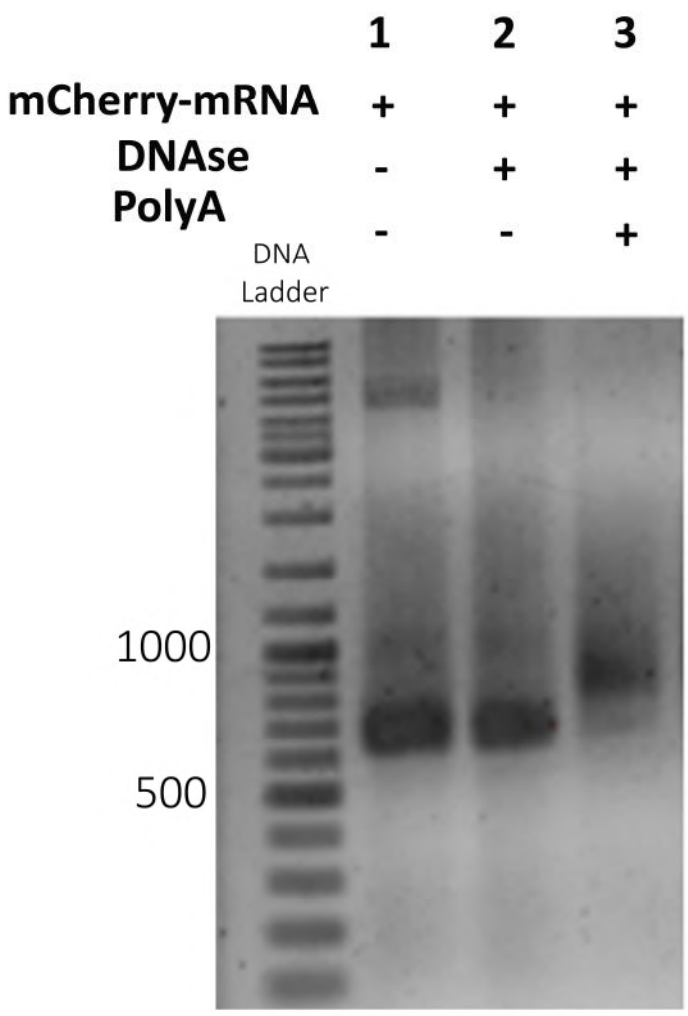

Supp Fig 1 ,Vilpreux et al 2023

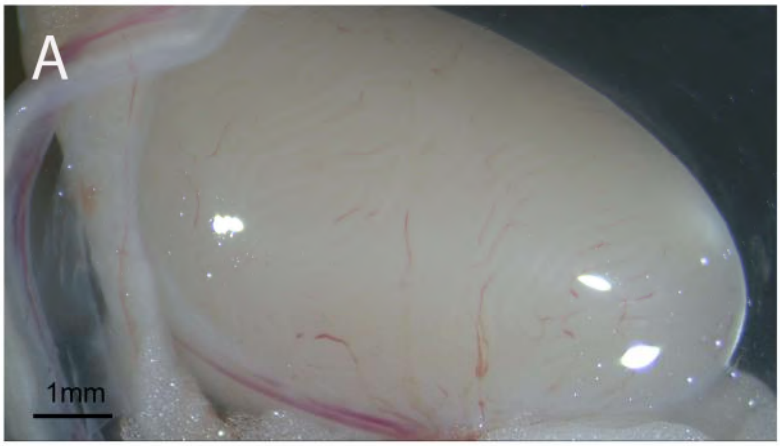

B

Pearly white lesions

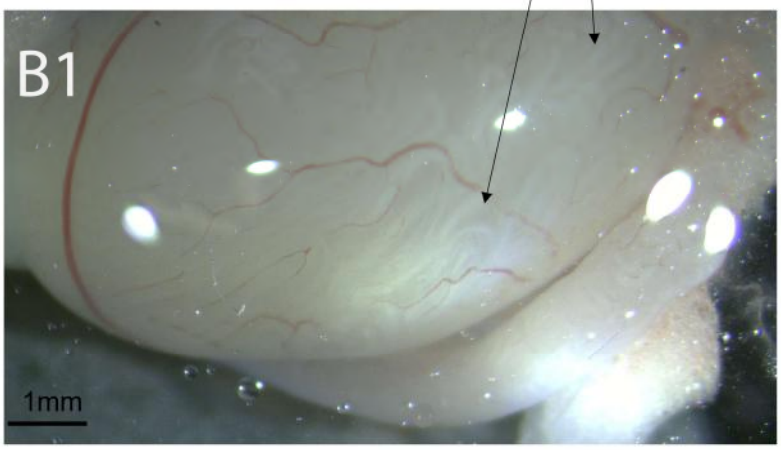

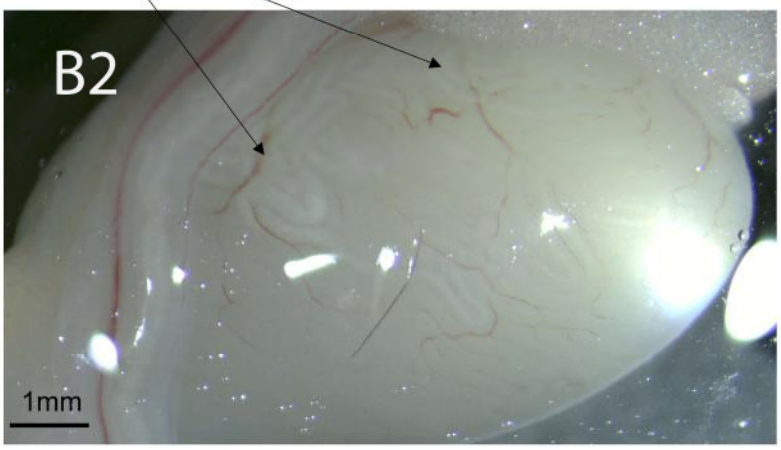

Supp Fig 2 , Vilpreux et al 2023

mCherry-mRNA

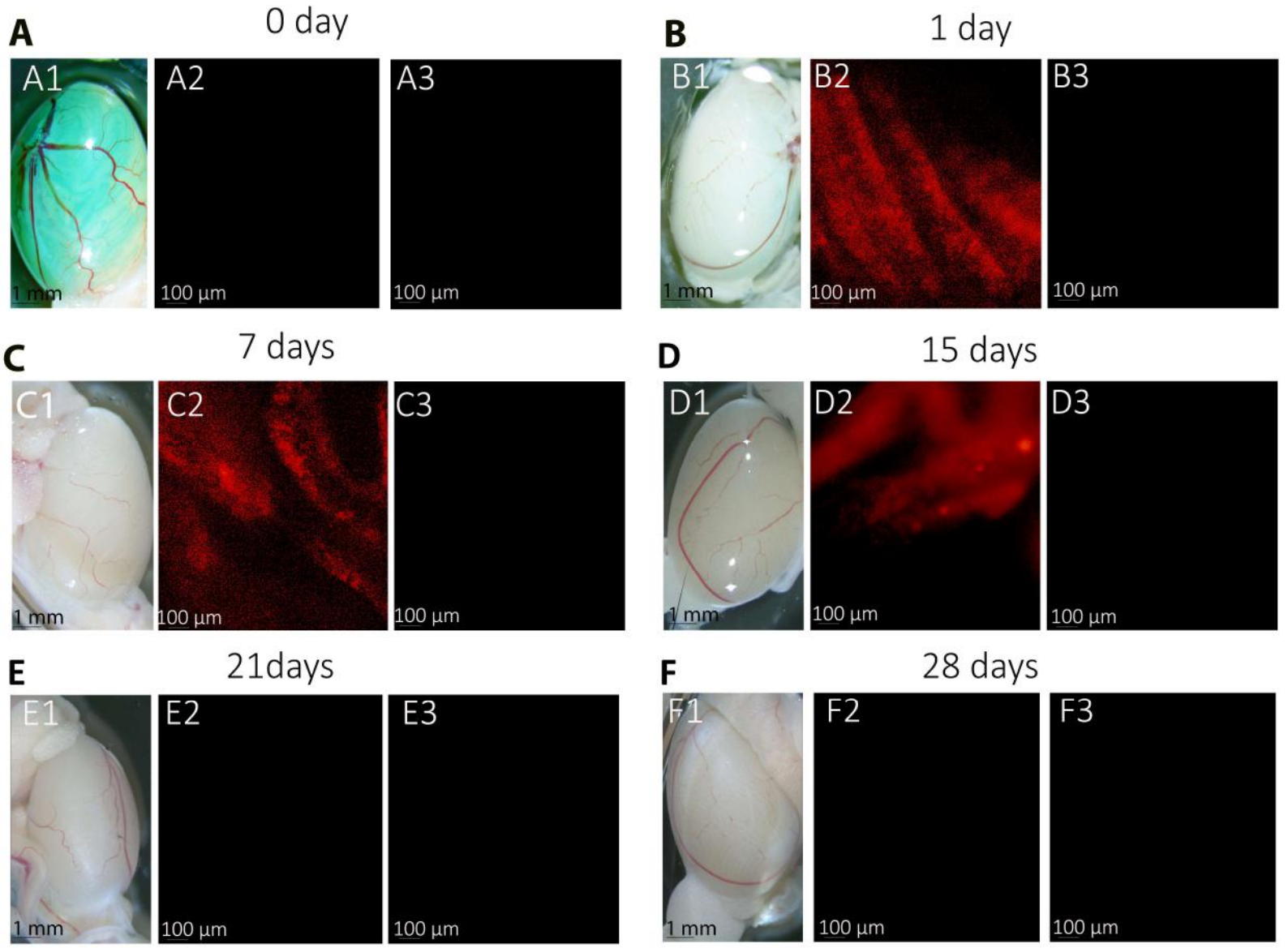

Supp Fig 3, Vilpreux et al 2023

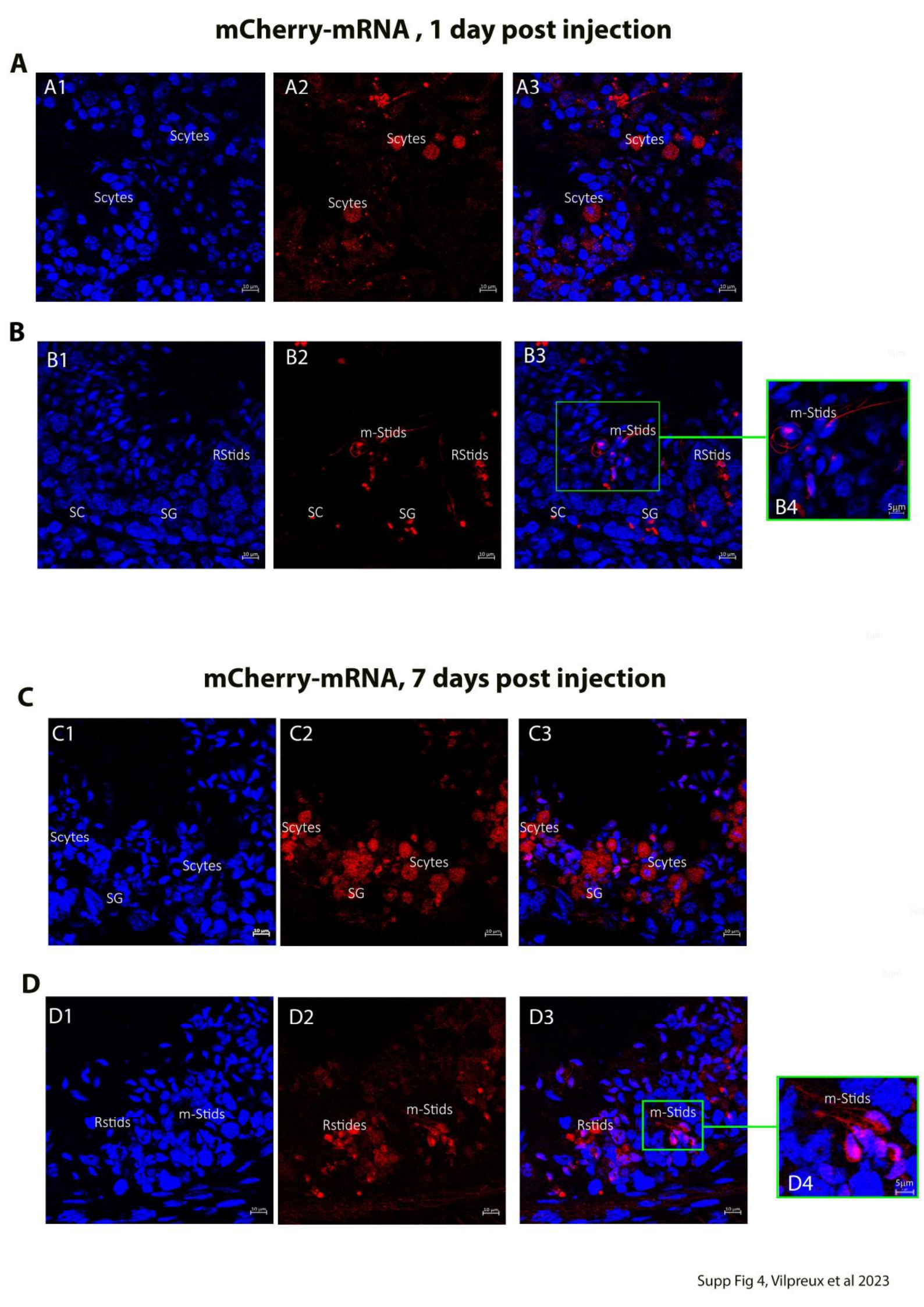

Supp Fig 4, Vilpreux et al 2023

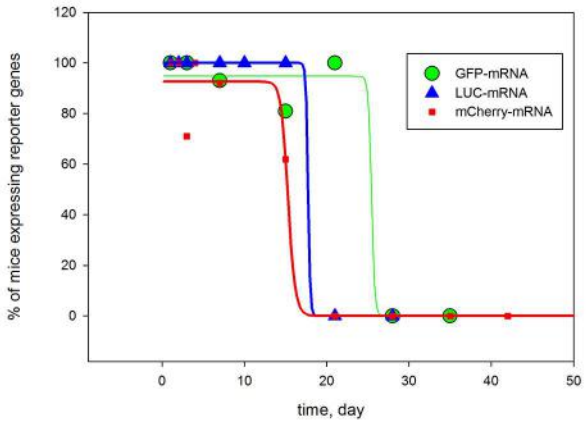

Supp Fig 5, Vilpreux et al 2023

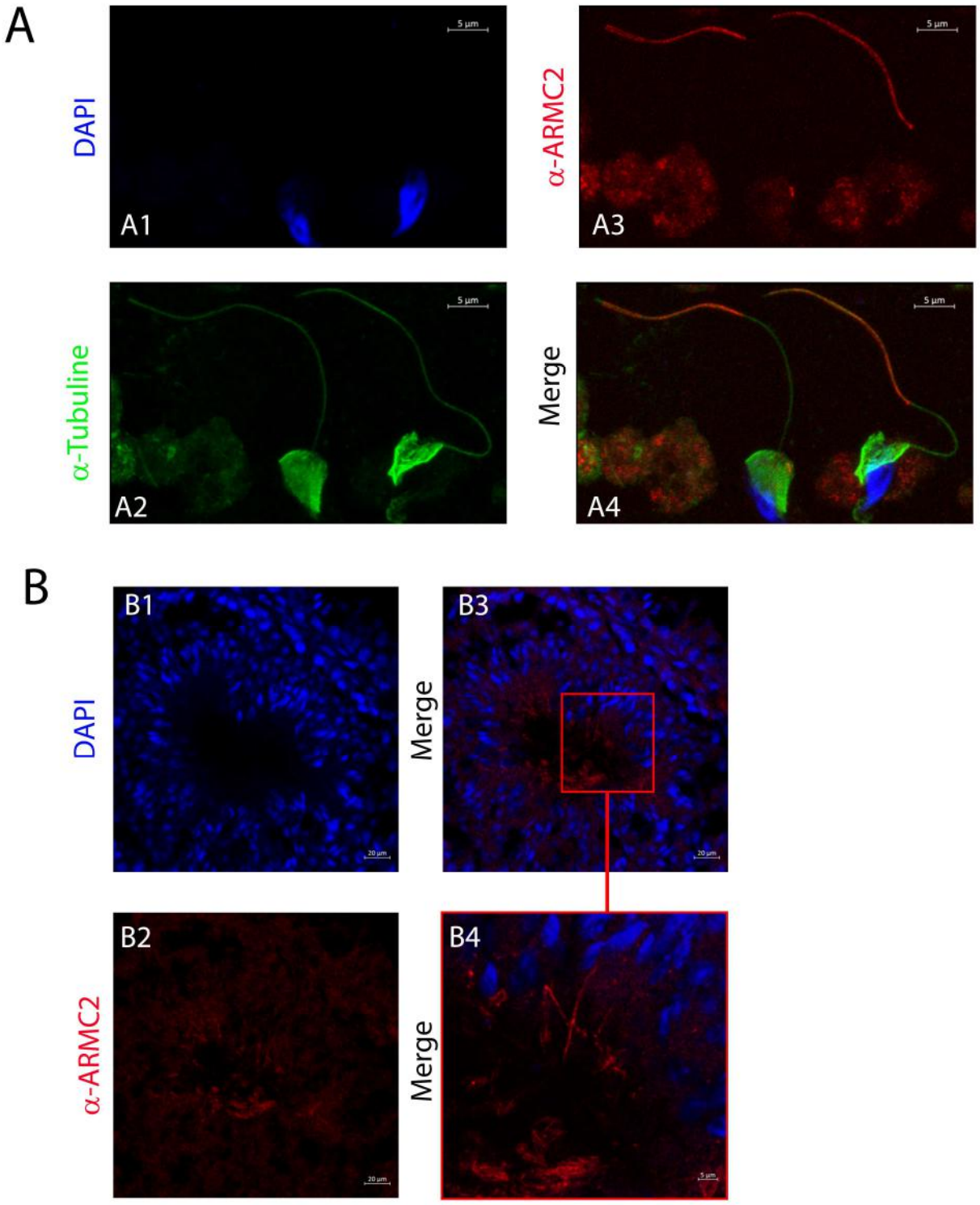

Supp Fig 6, Vilpreux et al 2023

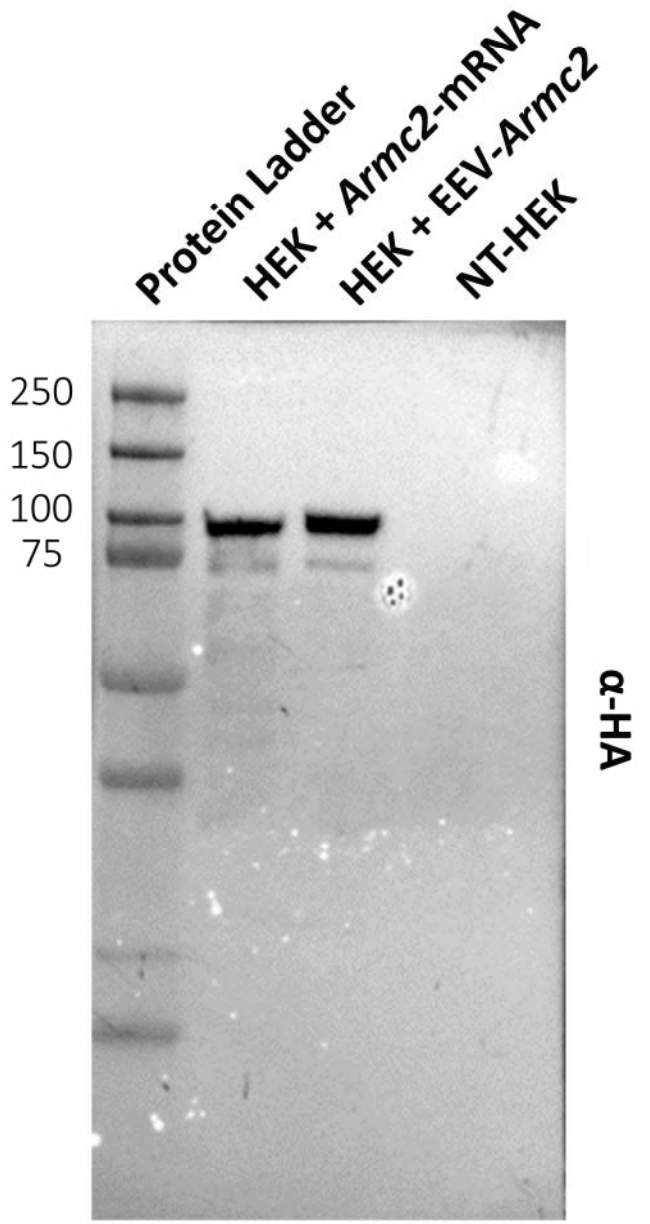

Supp Fig 7, Vilpreux et al 2023

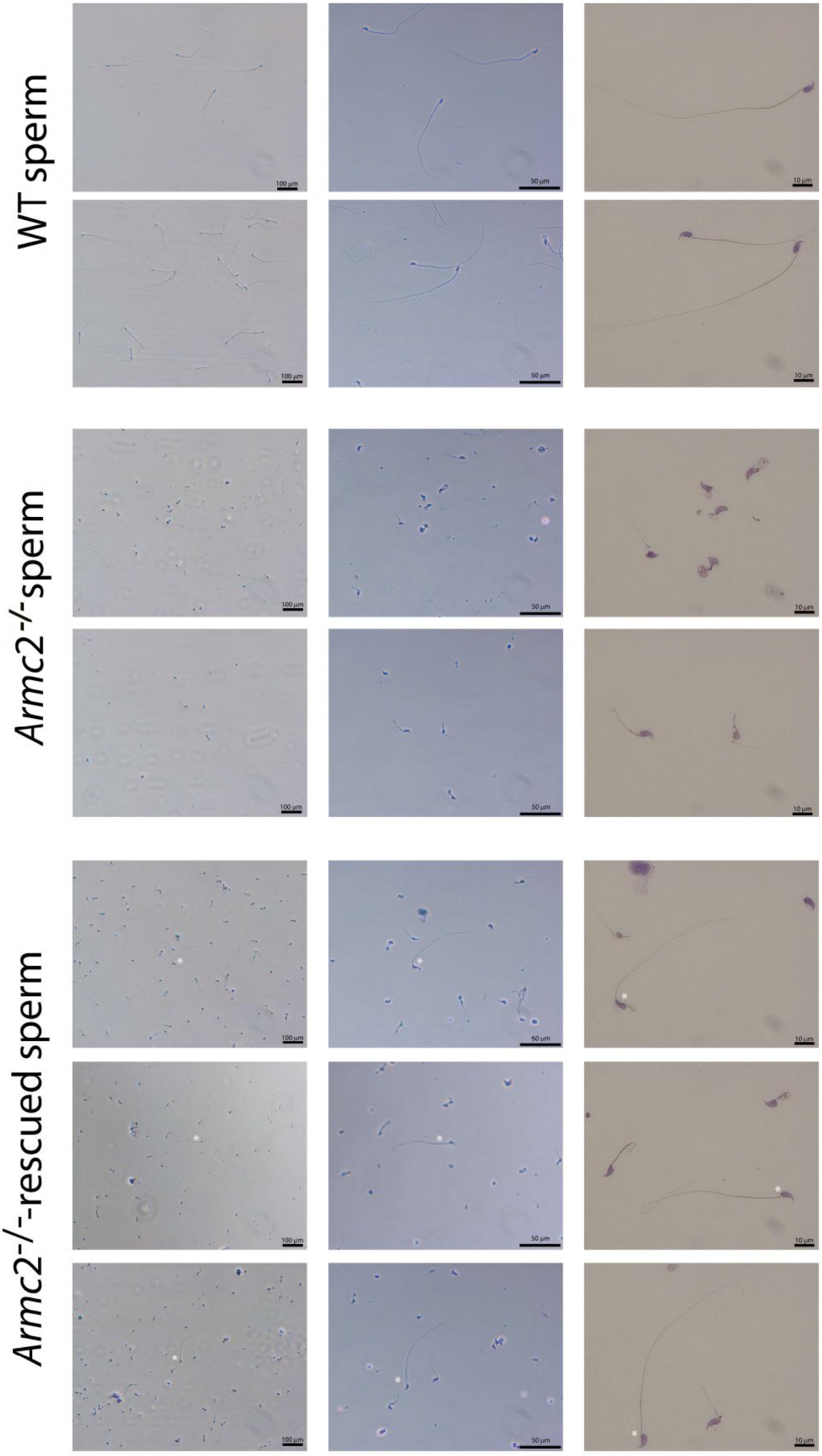

Supp Fig 8,
Vilpreux et al 2023

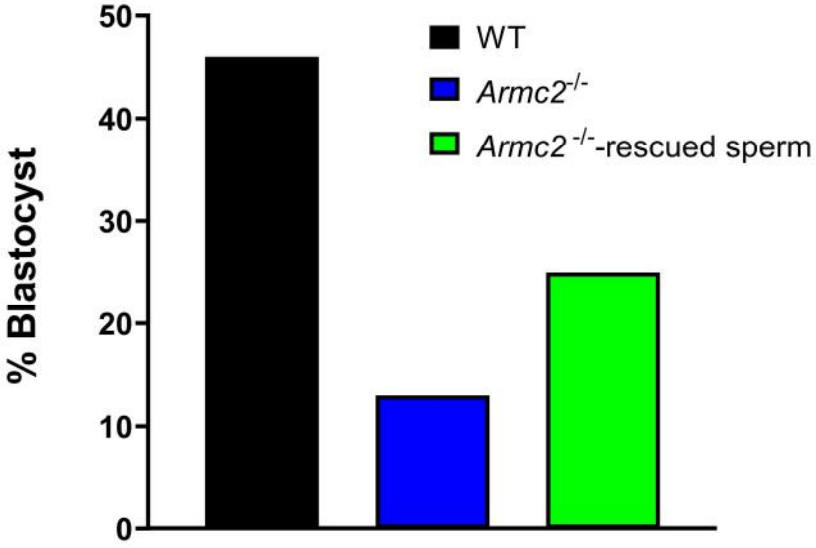

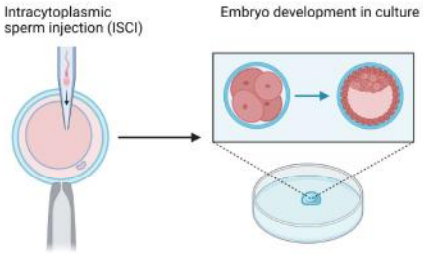

Supp Fig 9, Vilpreux et al 2023